Supporting Appendix

Supporting Materials and Methods.

Study samples. The UK Biobank is a large prospective study of over 500,000 individuals in the United Kingdom(UK)(1). Participants were 40-69 years of age during the recruitment phase (2006-2011). To avoid issues related to population structure, we studied only the 376,366 individuals of self-reported white-British ancestry. Unless otherwise notes we restricted our analysis to males over 50y old at assessment and females over 45y old, to ensure that number of children born to date is a good proxy for lifetime reproductive success. These filters resulted in 217,728 Female and 158,638 Male samples with phenotypic data. Of these individuals, there were 157,807 Female and 115,902 Male samples with genetic data available that were genetically unrelated (relatedness < 0.05).

Phenotypic data. The UKB contains data on the number of live births for females and the children fathered for males. These two variables were treated as life time reproductive success(LRS). To calculate relative lifetime reproductive success (rLRS) we followed the approach of (2). Briefly, the samples were split into birth cohorts and LRS values were divided by the cohort specific mean value. We calculated rLRS within 4 non-overlapping birth cohorts, based on birth year. Specifically, the birth cohorts are: Cohort 1 (1934-1942), Cohort 2 (1943-1948), Cohort 3 (1949-1955) and Cohort 4 (1956-1965). In all subsequent regression analyses age, birth cohort and data collection assessment center were treated as covariates. All phenotypes, except LRS, measured in the set of 376,366 post-reproductive white-British ancestry samples were split by sex and then scaled to mean zero and variance one. If a sample was measured on multiple visits to the assessment center then we used the mean value across measurements except in the case of educational attainment for which the maximum value was used. Unless otherwise noted, individuals more than 6 standard deviations from the mean were removed as outliers.

Genetic data. The UKB genetic data were collected using two similar genotyping arrays. Nearly 450,000 participants were genotyped on the custom Affymetrix UK Biobank Axiom® (UKBA) array, while an additional 50,000 participants were genotyped using the UK BiLEVE (UKBL) array. The two arrays have over 95% common marker content, with the UKBA array having a small number of additional markers for genome-wide coverage. The genetic data was imputed using two different reference panels, by the UK Biobank team. The Haplotype Reference Consortium (HRC) panel was used as first choice option, but for SNPs not in that reference panel the UK10K + 1000 Genomes panel was used. A problem arose in the second set of imputed data from the UK10K + 1000 Genomes panel. The genotypes at these SNPs are imputed correctly, but have not been recorded as having the correct genome position in the files. We have established that the imputed data from the HRC panel is not affected and has the correct positions. This is about 40M sites and will include the majority of the common SNPs i.e. sites most likely to show genetic associations. These sites are readily identified since the HRC site list is public. The sample of "White British" ancestry individuals was derived using principal component analysis and the self-reported ancestry information. For our further genetic analyses, we selected 1,162,900 HapMap3 SNPs with info score >0.3, minor allele frequency >=0.01 and Hardy-Weinberg Equilibrium test p-value >=1e-6. We further constructed genetic relatedness matrices in GCTA (3) and removed one of each pair of individuals with estimated SNP marker relatedness greater than 0.05 or if a genetically inferred gender of the sample did not match the self-reported gender. For some analyses only the UKB interim release was used which consisted of 108,402 unrelated White British individuals.

Phenotypic regression analyses. To estimate linear and quadratic selection gradients, we performed simple linear regressions of each phenotype and its square onto rLRS independently and through a multiple linear regression. In both cases, the phenotypes and their squared values were included and statistical significance was assessed by the Wald test.

The resulting regression coefficients are used to estimate the linear (β) and quadratic (γ) selection gradients (4, 5). The value of β is simply equal to the regression coefficient on the phenotype itself. However, the value of γ is twice the regression coefficient on the square of the phenotype (5).

The particular subset of phenotypes used in the multiple linear regression was chosen to reduce the variance of the regression estimates. We observed the phenotypic correlations between traits (Fig. S4 and S5) and noticed some sets of highly correlated traits. Within each set we prioritized inclusion in the final model by (1) significance of genetic correlation with rLRS, (2) significance of phenotypic regression on rLRS and (3) sample size. The UKB has very large sample sizes, but the missing data is non-overlapping for each trait. As such, the data matrix became singular upon inclusion of all trait interaction terms. Therefore, we only include the traits interaction with itself (the quadratic term). To further address multi-collinearity in the data we calculated the variance inflation factor (VIF) for each trait. Individual traits were removed from the model, starting with the trait with the highest VIF, and the VIF's were recalculated. This process was repeated until all VIF values were below 2 for all included traits.

Genetic correlation analyses. Summary statistic based LD-score regression(6, 7) was performed on the full UKB dataset to calculate genetic correlations between various traits and rLRS. GWAS summary statistics were generated using a simple linear association test in plink(8). Then, LD-score regression was performed using pre-computed LD-scores which are provided with the LD-score regression software.

In addition, a bivariate genetic variance component analysis was performed in the interim data release to establish genetic relationships between various traits and rLRS. The bivariate variance component model allows us to jointly estimate the genetic variance of each trait and their genetic covariance. Because of the large sample sizes of the UKB, BOLT-REML(9) was chosen for computational efficiency. Briefly, BOLT-REML estimates the genetic variance-covariance matrix via a Monte-Carlo Average

Information REML approach. The genetic variance parameters are initially estimated using the related BOLT-LMM(9), which is a Bayesian linear mixed model methods. BOLT-LMM assumes a mixture-of-normals prior on the SNP effects such that most SNPs have small effects and others may have large effects. Given the BOLT-LMM initial estimates, BOLT-REML then applies a rejection sampling technique to obtain final estimates of the genetic variance-covariance matrices. We assessed the statistical significance of the BOLT-REML genetic correlations via the Wald test.

SI Text.

BOLT-REML analysis of the interim UKB data release. We obtained genetic correlation estimates from a linear mixed modeling approach in addition to LD-score regression. Specifically, we used BOLT-REML, which gives very similar estimates to the standard gREML procedure in GCTA (10) but scales more efficiently with large sample sizes. Following (11) a REML estimate of the genetic correlation between traits and rLRS, $r_{g,rLRS}$, was directly estimated using common (MAF>0.01) SNP markers in a bivariate linear mixed model (LMM) approach (12, 13) using BOLT-LMM (9). The estimate of SNP heritability for rLRS varied across analyses and by sex. Due to the action of natural selection against deleterious mutations, the heritability of fitness components, such has reproductive success, is expected to be low and largely dominated by low frequency variants. Thus, our estimates of the common-SNP heritability of rLRS are most likely biased downward, which reduces the power of our genetic correlation analyses. Here we provide an overview of BOLT-REML results and a brief comparison to the LD-score regressions.

The BOLT-REML estimates of genetic correlation are summarized in Fig. S12. Many traits in females show a $\hat{r}_{g,rLRS}$ in the same direction as the phenotypic regression estimate $\hat{\beta}$. Overall, there was a strong positive correlation between the $\hat{\beta}$ and $\hat{r}_{g,rLRS}$ in females only (Fig. S15). Further, the total phenotypic correlation estimated from the mixed model is consistent with results from the regression analysis (Fig. S14 and table S3);see the following section for a more detailed discussion on the consistency between the phenotypic and genetic results.

In females, the median BOLT-REML estimate of $h^2_{SNP,rLRS}$ was 0.076, which on a relative scale is considerably larger than the value 0.0564 estimated from LD-score regression. While in males, the estimates of $h^2_{SNP,rLRS}$ from the two methods were quite close, with the BOLT-REML estimate being equal to 0.035 and the LD-score regression estimate being equal to 0.033. It is also known that, all else equal, LD-score regression estimates of genetic variance components will have larger standard errors than estimates obtained from mixed modeling approach. This means that there are multiple competing factors affecting power to detect non-zero genetic correlations including the sample size, the heritability explained by the model, and the precision of the estimate.

Four body-size related traits have a significant $\hat{r}_{g,rLRS}$ in females: WHR, WC, BFP and BMI. An additional two body-size traits, WT and HC were marginally significant in females. No traits show a significant $\hat{r}_{g,rLRS}$ at the FWER≤ 0.05 level in males, but $\hat{r}_{g,rLRS}$ for male BMI is marginally significant and in the same direction as the phenotypic result ($\hat{\beta}$). Again consistent with the phenotypic results, $\hat{r}_{g,rLRS}$ values for EA and AFB in females are significant and negative.

The BOLT-REML and LD-score regression estimates of $\hat{r}_{g,rLRS}$ were highly correlated. However, the specific traits which passed the study-wise significance threshold varied considerably. More male traits were significant in the LD-score regression analysis while the opposite was true for females and the BOLT-REML analysis. However, it is important to emphasize that significance thresholds are somewhat arbitrary and we draw attention to the overwhelming consistency of the estimates obtained from the two approaches as demonstrated by Fig. S13.

Consistency of phenotypic and genetic correlations. In the main text of this manuscript we present results from a phenotypic analyses in a large section of the UKB data and above we presented a genetic analysis from a reduced subset of that data. Specifically, we perform a linear regression for phenotypic analyses and bivariate linear mixed modeling for the genetic analyses. Here in this section we would like to provide a joint interpretation and discuss the issue of consistency between results of these two analyses. Below we provide calculations for various correlation coefficients obtained from our analyses; the empirical estimates of these coefficients are presented in table S3.

The $\hat{\beta}$ estimates from a linear regression can be expressed in terms of phenotypic covariances and correlations. In the model

$$rLRS = \beta P + \epsilon$$

we have

$$\begin{aligned}\hat{\beta} &= \frac{cov(P, rLRS)}{V(rLRS)} \\ &= r_p \frac{\sigma_{rLRS}}{\sigma_P}\end{aligned}$$

Where r_p is the phenotypic correlation coefficient in the sample. Therefore, we obtain by simple algebra the first expression for the phenotypic correlation coefficient directly from our phenotypic analyses, which we call $r_{p,1}$.

$$r_{p,1} = \hat{\beta} \frac{\sigma_P}{\sigma_{rLRS}}$$

Given some assumptions we can obtain a similar expression for phenotypic correlation from the genetic results. We assume an additive polygenic model for both traits (P and $rLRS$) analyzed in the bivariate model such that the traits are expressed as additive genetic and environmental components.

$$rLRS = A_{rLRS} + E_{rLRS}$$
$$P = A_P + E_P$$

We can then further decompose the additive genetic component into a portion explained by genotyped SNPs and a remainder.

$$A_{rLRS} = A_{s,rLRS} + A_{r,rLRS}$$
$$A_P = A_{s,P} + A_{r,P}$$

The covariance between $rLRS$ and P is

$$\begin{aligned} cov(rLRS, P) =& cov(A_{rLRS}, A_P) + cov(E_{rLRS}, E_P) \\ cov(rLRS, P) =& cov(A_{s,rLRS}, A_{s,P}) + \\ & cov(A_{r,rLRS}, A_{r,P}) + cov(E_{rLRS}, E_P) \end{aligned}$$

From the bivariate linear mixed model we obtain estimates of the correlation between the additive genetic components of both traits explained by SNPs and the covariance between the residual components.

$$r_{s,g} = \frac{cov(A_{s,rLRS}, A_{s,P})}{\sqrt{V(A_{s,rLRS})V(A_{s,P})}}$$
$$r_{s,e} = \frac{cov(A_{r,rLRS} + E_{rLRS}, A_{r,P} + E_P)}{\sqrt{V(A_{r,rLRS} + E_{rLRS})V(A_{r,P} + E_P)}}$$

We cannot assume that the environmental components of the two phenotypes is zero ($cov(E_{rLRS}, E_P) = 0$) because this is a strong untested assumption and it is one that would not be true under a causal relationship between P and $rLRS$. Therefore, it is not possible to extrapolate from the mixed model results to the true full genetic correlation (r_g). However, we can provide a second calculation of the full phenotypic correlation from the genetic results which we call $r_{p,2}$.

$$\begin{aligned} r_{p,2} &= \frac{cov(rLRS, P)}{\sqrt{V(rLRS)V(P)}} \\ &= \frac{cov(A_{s,rLRS}, A_{s,P}) + cov(A_{r,rLRS} + E_{rLRS}, A_{r,P} + E_P)}{\sqrt{V(rLRS)V(P)}} \\ &= \frac{r_{s,g}\sqrt{V(A_{s,rLRS})V(A_{s,P})}}{\sqrt{V(rLRS)V(P)}} \\ &+ \frac{r_{s,e}\sqrt{V(A_{r,rLRS} + E_{rLRS})V(A_{r,P} + E_P)}}{\sqrt{V(rLRS)V(P)}} \end{aligned}$$

The two calculations of phenotypic correlation should be closely related as one is obtained using a subset of the data used from the other. Indeed in a regression of $r_{p,1}$ on $r_{p,2}$ the $R^2 = 0.94$ (Fig. S14). The residual variance-covariance estimates from the bivariate model contain both untagged genetic and non-genetic effects. Therefore we can not definitively demonstrate consistency between the pure phenotypic and genetic results. However, we can ask how well the phenotypic correlations predict the genetic correlations. To do so we regressed the mixed model genetic correlation estimates $r_{s,g}$ onto the phenotypic correlation estimates from the phenotypic regressions $r_{p,1}$. The regression coefficient in that model was 2.96 with an adjusted $R^2 = 0.27$. In other words the phenotypic correlation values explain 27 percent of the variance in genetic correlation estimates.

Correlation between rLRS and a polygenic predictor for height. As an alternative approach to finding genetic evidence for a relationship between rLRS and height we constructed a polygenic predictor for height based on a meta-analysis of published height GWAS and the interim UKB data. This meta-analysis has an effective sample size of 390,000. From the meta-analysis there were 1,371 SNPs that passed a clumped p-value threshold hold of 10^{-6}. We predicted height in the UKB samples using the sample genotypes and estimated effect sizes at these 1,371 SNPs. Our predictor explains 25 percent of phenotypic for height(Fig. S22).

The rLRS values were regressed onto the predicted height and squared height values for males and females separately. In males neither the linear nor quadratic predictor were significantly associated with rLRS. However, in females both the linear and the quadratic predictor showed marginal significance. In females, the estimated effect size of the height predictor on rLRS was $-0.0081 \pm 0.004 (p = 0.0624)$ and effect size of the squared height predictor on rLRS was $-0.007919 \pm 0.003 (p = 0.0097)$. This result is qualitatively consistent with our phenotypic observations of a weak directional and quadratic relationship between rLRS and height.

We performed a simulation to better understand the behavior of the polygenic predictors for height and their relationship to rLRS. We simulated fitness values under a model of multivariate stabilizing selection(14) where three phenotypes contribute to fitness. One of the three underlying phenotypes was treated as being under directional selection by setting the phenotypic optimum to be different from 0 for that phenotype only.

We simulated genotypes at 20,000 unlinked biallelic variants. 10,000 of these variants were causal for the phenotype under directional selection. Variant effect sizes were estimated in a panel of 300,000 individuals using a simple linear association test. Using the estimated variant effects we created polygenic predictors for the phenotype and squared phenotype in an independent validation panel of 50,000 individuals. The predictors were regressed against the simulated fitness values in the independent validation panel.

The simulations recapitulate an important qualitative signature of our empirical polygenic predictors. As the number of SNPs in the predictor is increased the p-value of a predictor goes down and then eventually goes back up(Fig. S23. When the number of SNPs is too low, there is no statistical power to predict in a new panel. However, if too many SNPs are included then we are adding noise to the predictor and power is reduced. This effectively reflects a transition from a model that under-fits to one that has over-fit the data; both under and over fitting reduce prediction accuracy in an independent dataset.

According to our simulations, the transition from under-fitting to over-fitting as a function of number of variants happens much faster for the quadratic predictor than for the linear predictor. This is likely due to the propagation of measurement error through a quadratic function. By predicting the variant effects on the phenotype and then predicting its square we have propagated the error of the variant effect size estimates.

Mendelian randomization using summary statistics for Educational Attainment. We use Mendelian randomization based on summary statistics (GSMR) (15) to assess the evidence for a possible causal relationship between educational attainment and reproductive phenotypes. In the main text of this manuscript we show that there is a strong phenotypic and genetic correlation between educational attainment and relative lifetime reproductive success. Briefly, a Mendelian randomization (MR) analysis estimates and tests a causal relationship of trait X on trait Y by using known SNP associations for trait X as instruments. The rationale is that if trait X causes Y then any perturbation that affects X will have the same proportional effect on Y.

Using summary statistics from GWAS for educational attainment (16) and the UKB data on rLRS used in the main text, we tested the hypothesis that educational attainment, or a trait genetically highly correlated with it, is causal for rLRS. Using 50 instruments (genome wide significant SNPs for educational attainment) we estimate that $\hat{\beta_{EA,rLRS}} = -0.2 (p < 10^{-5.8})$.

This instrument variable analysis implies that an increase of one standard deviation in educational attainment leads to a 0.2 decrease in rLRS. While this limited analysis is insufficient to fully demonstrate causality, the results are clearly consistent with the hypothesis that educational attainment, or a trait such as cognitive ability (which is genetically correlated with EA and might itself be causal for EA), has a negative causal relationship with lifetime reproductive success.

We also performed a similar GSMR analysis between educational attainment and age at first birth. Using the same educational attainment summary statistics, we had 51 instruments and estimated that $\hat{\beta_{EA,AFB}} = 0.653 (p < 10^{-21})$. The results are consistent with the hypothesis that educational attainment (or a highly correlated trait) causally increases age at first birth.

Linear regression sensitivity analysis. The phenotypic results presented in the main text followed the default data filter and QC pipeline. In the defaults pipeline we used age cutoff of 50 and 45 for males and females respectively, did not perform inverse noram transformation on the data, used 6 standard deviations to define outliers for removal and did not remove known related individuals. We were concerned that, while rare, it is possible for males and females to have children above the ages of 50 and 45 respectively. When the age inclusion thresholds were increased to 55 and 50 for males and females respectively, we did not see many major changes to the results although the specific magnitudes of the selection gradient estimates did change. Similarly, we increased stringency of the outlier inclusion criteria by removing individuals outside of 4 standard deviations from the mean. The increased outlier stringency had little qualitative effect on the our results.

We found that our results were also robust to normalization via inverse-normal transformation and the removal of known related individuals (Fig. S20 and S21). Additionally, a logistic regression analysis was performed using a binary encoding of LRS in which zero indicates no children and one indicates one or more children. Many of the phenotypes appear to be associated with this binary phenotype. This indicates that some of the our phenotypic regression results can be explained by whether people end up having children or not. These results are contained in Dataset S1 along with all other regression results.

The broad sense heritability of a squared phenotype. In the main text, we argue that the narrow sense heritability for a squared trait will necessarily be much lower than the heritability for the trait itself. This stems from a few fundamental features of the squared phenotype including gene-by-environment interactions, over-dominance and epistasis. We will not derive the general case here, but instead will illustrate a couple of informative special cases. First, we will demonstrate the reduction in broad-sense heritability for a general trait with independent genetic and environmental components. Second, we will derive the dominance and epistatic variance components under purely additive single-locus and two-locus trait models. We finally appeal to our empirical results to support our claim (Fig. S19).

We begin with the simple phenotypic model with independent genetic and environmental components.

$$P = G + E$$
$$H^2 = \frac{V(G)}{V(P)} = V(G)$$

Where $P \sim \mathcal{N}(0,1)$, $G \sim \mathcal{N}(0, V(G))$, and $E \sim \mathcal{N}(0, V(E))$. Assume that G and E are independent. Therefore when we take the squared phenotype we get:

$$P^2 = G^2 + 2GE + E^2$$

I want to find expressions for $V(P^2)$, $V(G^2)$, $V(E^2)$, and $V(2GE)$. Because G and E both have mean zero and are independent:

$$V(2GE) = 4V(G)V(E)$$

From the definition of variance:

$$V(X^2) = E(X^4) - E(X^2)^2$$

This is the difference between the fourth central moment and the square of the second central moment. For a normal random variable the fourth central moment is 3 times the squared variance

$$\mu_4 = 3\sigma_X^4$$
$$V(X^2) = 3\sigma_X^4 - (\sigma_X^2)^2$$
$$V(X^2) = 2(\sigma_X^2)^2$$

The remaining expressions clearly follow.

$$\sigma_P^2 = 1$$
$$\sigma_G^2 = V(G) = H^2$$
$$\sigma_E^2 = V(E) = 1 - H^2$$

Therefore:

$$V(P^2) = 2$$
$$V(G^2) = 2(H^2)^2$$
$$V(E^2) = 2(1 - H^2)^2$$
$$V(GE) = 4 * H^2(1 - H^2)$$

If we decompose the squared phenotype, we can get expressions for the proportions of variance due to each component:

$$\frac{V(G^2)}{V(P^2)} = (H^2)^2$$
$$\frac{V(E^2)}{V(P^2)} = (1 - H^2)^2$$
$$\frac{V(2GE)}{V(P^2)} = 2 * H^2(1 - H^2)$$

Thus the broad sense heritability of squared phenotype will be the square of broad sense heritability of the phenotype.

Finite locus models for a squared phenotype. Next, we will show how the genetic variance for the squared trait decomposes under single and two locus models of a trait. Consider a single biallelic locus contributing to purely additive trait P with alleles and at frequencies p and q respectively.

	A_1A_1	A_1A_2	A_2A_2
G	a	0	$-a$
G^2	a^2	0	a^2
G^{2*}	0	$-a^2$	0

The additive variance in P is given by the classic formula.

$$V_{G^2}(A) = 2pqa^2$$

In the case of the P^2 there is no additive effect, but there is a dominance deviation ($d = -a^2$) such that:

$$V_{G^2}(A) = 2pq(-a^2(q-p))^2$$
$$V_{G^2}(D) = (-2pqa^2)^2$$

$$\frac{V_{G^2}(A)}{V_{G^2}(A) + V_{G^2}(D)} = \frac{2pq(-a^2(q-p))^2}{2pq(-a^2(q-p))^2 + (-2pqa^2)^2}$$
$$= \frac{a^2(q-p)^2}{a^2(q-p)^2 + 2pqa^2}$$
$$= \frac{1}{1 + \frac{2pq}{(q-p)^2}}$$

The expression for the percent of total genetic variance which is due to additive effects only depends on the allele frequencies .The absolute magnitude of the additive variance for the squared genetic component is maximized for $p = 0.5 \pm \frac{1}{2\sqrt{2}}$. However, the relative magnitude of the of the additive component is maximized as p goes to zero. This composition of the genetic variance across the range of allele frequencies is shown in Fig. S16. Thus, for a given trait architecture the additive component of squared trait will be more highly influenced by rare variants. This fact further reduced the power of present study, in which we use common SNPs to estimate genetic relatedness.

To illustrate the inclusion of epistasis, we derive the variance components under a two-locus model with equal additive effects. The loci have equal effects, a, and allele frequencies p_1 and p_2.

The genetic values for the trait and the squared trait are

$$G = \begin{pmatrix} 2a & a & 0 \\ a & 0 & -a \\ 0 & -a & -2a \end{pmatrix}$$

$$G^2 = \begin{pmatrix} 4a^2 & a^2 & 0 \\ a^2 & 0 & a^2 \\ 0 & a^2 & 4a^2 \end{pmatrix}$$

For this model, we follow the approach of Kojima (17) for the derivation of genetic variance components based on partial derivatives of the population mean with respect to allele frequencies. Given the population mean genetic value μ, the (L-additive X Q-dominance) variance due to a particular locus of set of loci can be defined as:

$$a_{LQ} = \frac{1}{2^{L+Q}} \frac{\delta^{L+2Q}\mu}{\prod_i^L \delta p_i \prod_j^Q p_j^2}$$
$$\sigma^2_{LQ} = 2^L \prod_i^L p_i(1-p_i) \prod_j^Q (p_j(1-p_j))^2 a^2_{LQ}$$

For example, the additive variance for a trait with M loci would be found by setting L=1 and Q = 0, such that:

$$a_{10,i} = \frac{1}{2}\frac{\delta\mu}{\delta p_i}$$
$$\sigma^2_{10} = \sum_i^M 2p_i(1-p_i)a^2_{10,i}$$

In the case of our two locus squared trait model, we will have additive, dominance and additive by additive epistatic terms. It can be shown that dominance interactions go to zero, i.e DxA and DxD epistasis.

$$\begin{aligned}\mu_{G^2} =& 4a^2(1-p_2)^2(1-p_1)^2 + 2a^2(1-p_2)p_2(1-p_1)^2 + \\ & 2a^2p_1(1-p_2)^2(1-p_1) + 2a^2p_1p_2^2(1-p_1) + \\ & 4a^2p_1^2p_2^2 + 2a^2p_1^2 + (1-p_2)p_2\end{aligned}$$

$$V_{G^2}(A) = \sum_{i=1}^2 2p_i(1-p_i)\frac{\delta\mu_{G^2}}{\delta p_i}$$
$$V_{G^2}(D) = \sum_{i=1}^2 (p_i(1-p_i))^2 \frac{\delta^2\mu_{G^2}}{\delta p_i^2}$$
$$V_{G^2}(AA) = 4p_1(1-p_1)p_2(1-p_2)\frac{\delta\mu_{G^2}}{\delta p_1 \delta p_2}$$

In Fig. S17, we illustrate how much of the total genetic variance is attributable to the additive component across the allele frequencies at each locus. The conclusions are similar to the single locus model: at intermediate allele frequencies there is a substantial reduction in the relative contribution of additive variance to total genetic variance for a squared phenotype. This implies that, even if the additive variance is preserved at some loci, our study using common variants will be severely under powered. However, as the number of loci in the model increase, the importance of the additive variance component should also increase (18). Regardless, our empirical results show that narrow-sense heritability of a squared trait is severely reduced compared to that of the trait itself.

Additive heritability of a squared trait under a polygenic model. In the previous section, we derived estimates of genetic variance under one and two locus model. However, the traits studied in this work are highly polygenic and we sought an alternative approximation based on the infinitesimal model. Under the infinitesimal model, we can approximate the additive heritability of a trait as the limit of the correlation between relatives as the correlation goes to zero(unrelated). This approximation should remain valid for functions a traits.

Let there be a phenotype Y which is purely additive and another phenotype $Z = Y^2$. We then consider both phenotypes Y and Z in a set of relatives with relatedness r for

$$\begin{aligned} Y &= A + E \\ E[Y] &= 0 \\ var[Y] &= 1 \\ Z_1 = Y_1^2 &= (A_1 + E_2)^2 \\ Z_2 = Y_2^2 &= (rA_1 + E_2)^2 \\ var[Z] &= 2 \end{aligned}$$

First, we need to derive a statement for the covariance between Z_1 and Z_2. Given that we $E[Y] = 0$, this derivation is relatively straightforward. The results follow below.

$$
\begin{aligned}
cov(Z_1, Z_2) &= 2r^2 V(A)^2 \\
\frac{cov(Z_1, Z_2)}{V(Z)} &= corr(Z_1, Z_2) = r^2 (h_Y^2)^2 \\
\lim_{r \to 0} \frac{corr(Z_1, Z_2)}{r} &= h_Z^2 \\
h_Z^2 = \lim_{r \to 0} \frac{corr(Z_1, Z_2)}{r} &= \lim_{r \to 0} r(h_Y^2)^2 = 0
\end{aligned}
$$

Therefore, under a highly polygenic model we expect there to be no additive genetic variance for a squared phenotype. To check this result we performed simple simulations in R. We sampled genotypes at M markers for N individuals (N>>M), assuming equal allele frequencies as allelic effects at each marker. Then we estimated the additive genetic variance using the R^2 from simple linear regression. We performed the regression on either the raw phenotypes or the phenotypes scaled to mean zero and variance one. Fig. S18 shows that the two locus analytical expression for additive variance is accurate when M=2 in a regression on the raw phenotypes. Fig. S18 also shows that when the phenotypes is scaled, the additive variance decreases rapidly as M (the number of markers) increases. From this we infer that, in accordance with our derivation under a polygenic model, as M gets very large there is no additive genetic variance for a squared phenotype.

Genetic control of variability. We first considered the behavior of the broad sense heritability of the square of a trait and found that it is the square of the broad-sense heritability of the trait. Next we derived expressions for genetic variance components under finite locus models following the classic approach of Kojima (17) (revisited in (18)). Our single locus derivations here are equivalent to those done by Yang, et al. (10). The finite locus models suggested that for a purely additive trait, the additive genetic variance of the square of trait will be less than genetic variance by an amount which depends on allele frequencies and number of loci. Under an infinitesimal model, based on the correlation between relatives, we expect there to be zero additive genetic variance for the square of a trait. Using simple simulations we validate our finite locus expressions and show that as the number of loci increases the additive genetic variance approaches zero, in agreement with the derivations under the infinitesimal model (Fig. S18).

Further, without making assumptions about the genetic architecture of the trait, any observed additive genetic variance for a squared phenotype can not be easily disentangled from the effects of loci that explicitly control phenotypic variability. In other words, when genotypic classes differ in phenotypic variability there will additive genetic variance for the square of the phenotype–a fact that has been previously appreciated in the literature(19–24).Yang et al (10) showed that it is possible to determine whether the additive effect of a SNP on the square of the trait is too large to be induced by that SNPs direct effect on the trait. However, this approach does not easily allow us to interpret variance components of the square of the trait, because of the confounding effect of the number of loci–we cannot say exactly what the heritability of the square of a purely additive trait should be without knowing both the heritability of the trait and the number of loci involved.

Converting from scaled phenotype to real phenotype estimates. For us to interpret out regression estimates in term of theoretical parameters, we scaled all phenotypes to mean zero and unit variance. However, for visualization of the predicted relationship between real phenotypes and rLRS, we must convert our regression estimates back to the real scale. While this is relatively straight forward algebra, the presence of the squared term add some minor additional complexity, which we illustrate here.

Given a sample of paired rLRS and trait values y and x, we convert x to z-scores:

$$z = \frac{x - x_0}{\sigma_x}$$

We have the multiple linear regression model:

$$y = \beta_0 + \beta_1 z + \beta_2 z^2 + \epsilon$$

$$y = \beta_0 + \beta_1 (\frac{x - x_0}{\sigma_x}) + \beta_2 (\frac{x - x_0}{\sigma_x})^2 + \epsilon$$

$$y = (\beta_0 - \frac{x_0 \beta_1}{\sigma_x} + \frac{\beta_2 x_0^2}{\sigma_x^2}) + (\frac{\beta_1}{\sigma_x} - \frac{2\beta_2 x_0}{\sigma_x^2}) x + \frac{\beta_2}{\sigma_x^2} x^2 + \epsilon$$

$$y = \beta_0^* + \beta_1^* x + \beta_2^* x^2 + \epsilon$$

SI Figures.

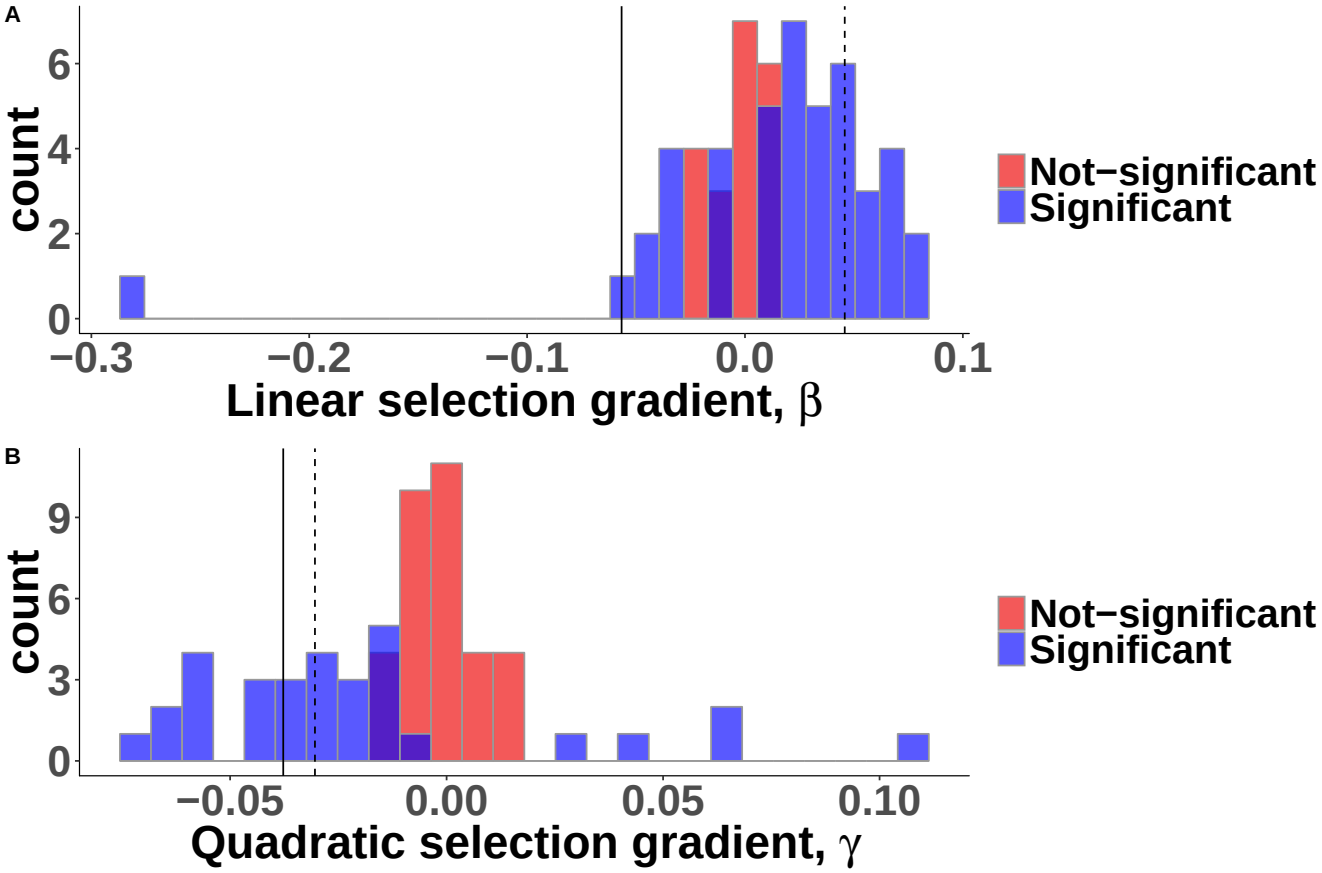

Fig. S1. Histograms showing the distributions of (A) linear and (B) quadratic selection gradients estimated from single trait regressions. Results are not split by sex, i.e. each data point is a result for a specific sex-trait pair. Linear selection gradients are equal to the regression coefficients estimates. Quadratic selection gradients are equal to twice the value of the regression coefficient estimates. A significance cut-off of FWER≤ 0.05 (Bonferroni correction) was chosen for visualization. Vertical lines show the values for Female (solid) and Male (dashed) height.

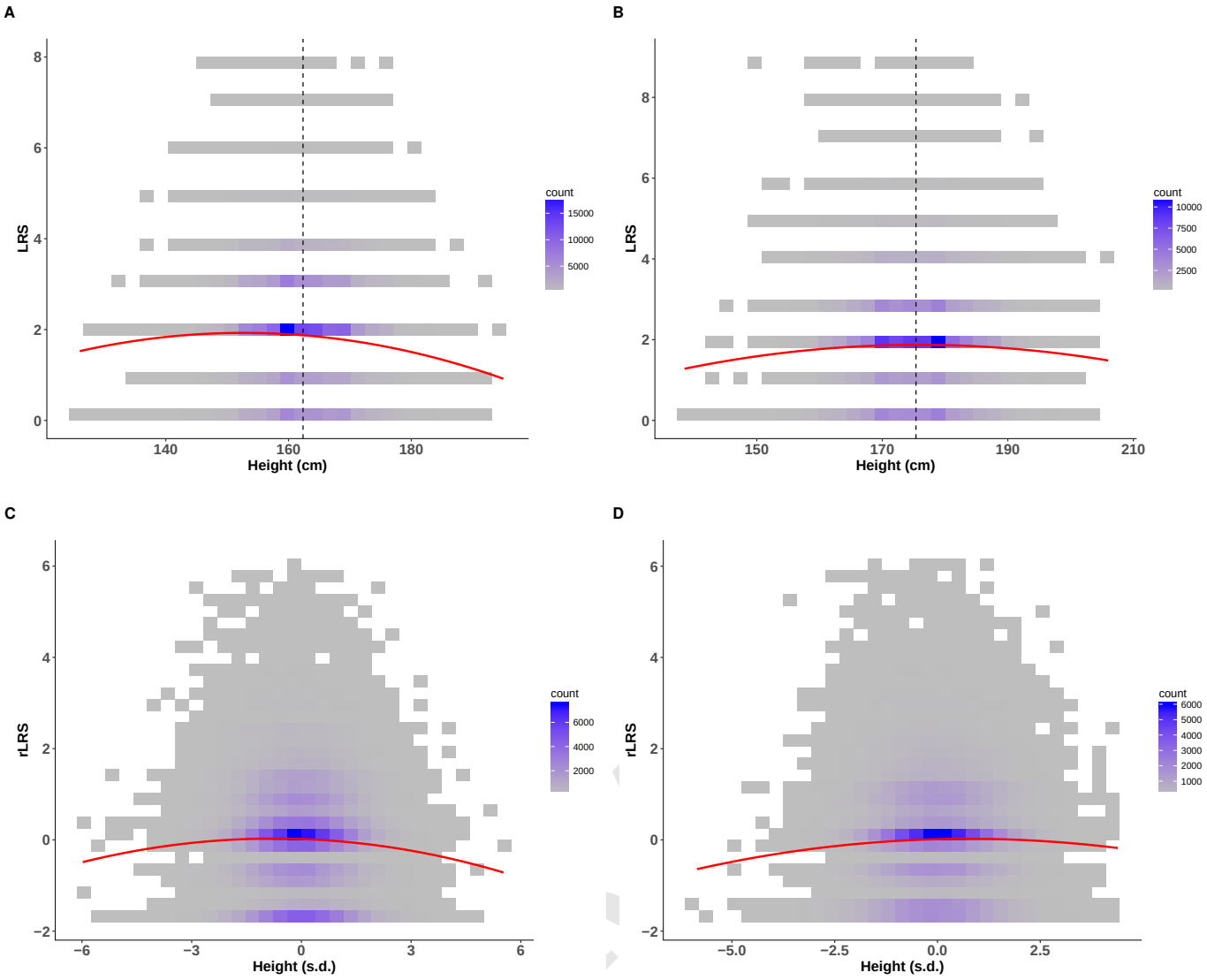

Fig. S2. Empirical relationships between LRS and Height. (Top row) Raw LRS values plotted against raw height values with a quadratic regression line fit to the data for (A) Females and (B) Males with a dashed horizontal line at the sex-specific population mean. (Bottom row) rLRS adjusted for age, birth cohort and assessment center values plotted against centered and scaled height values with a quadratic regression line fit to the data for (C) Females and (D) Males.

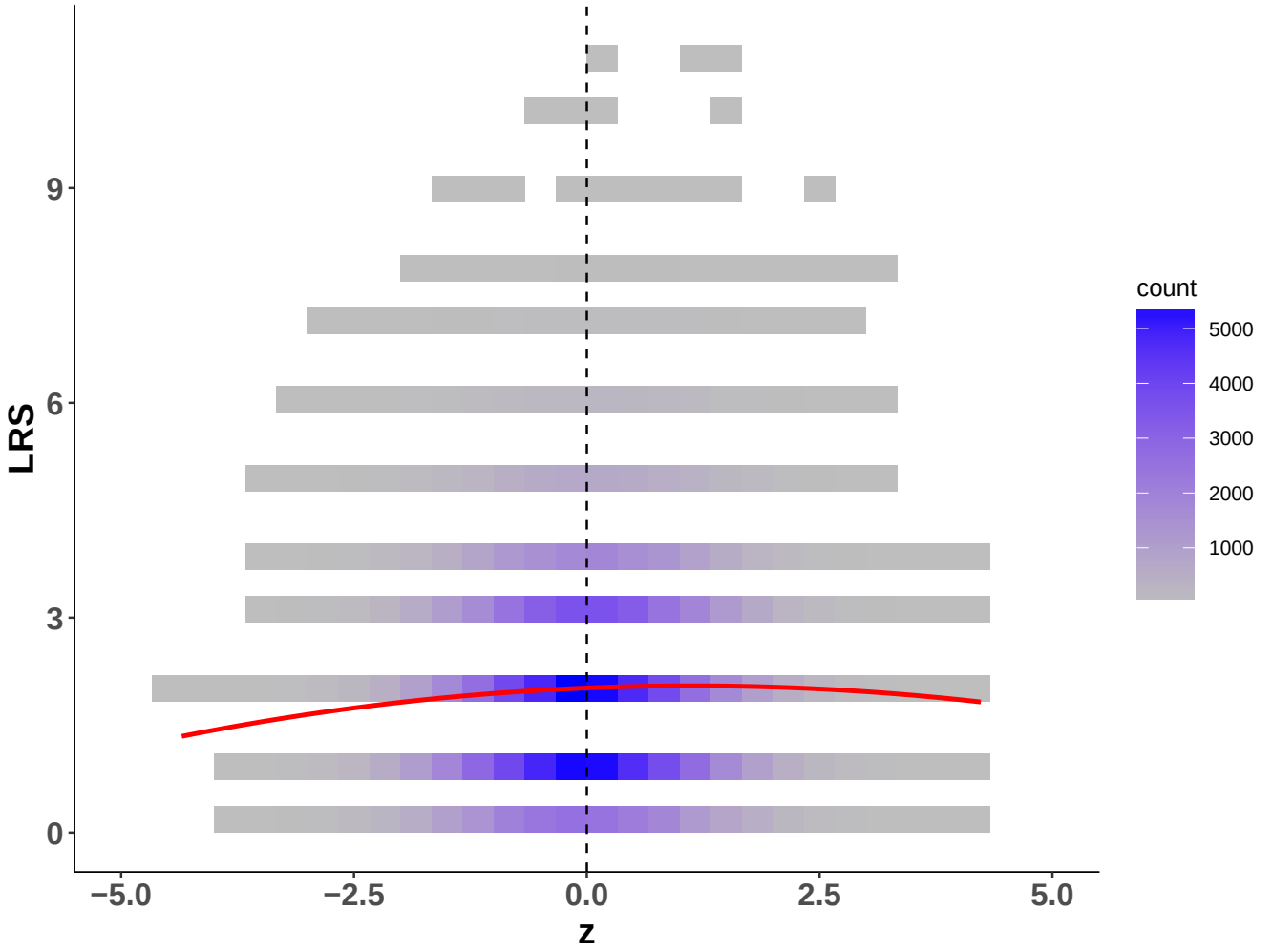

Fig. S3. Simulated relationship between LRS and a trait under stabilizing selection. Trait values for 150,000 individuals were drawn from a unit normal distribution. Fitness values were calculated with a Gaussian stabilizing selection fitness model with an optimum at $z_{opt} = 1$ and $V_s = 40$. Then LRS values were drawn from a poisson distribution with a mean equal to twice the relative fitness of each individual. We use twice the relative fitness so that the mean number of offspring per individual is 2, reflecting a constant population size in a sexual system. This poisson model for LRS will closely approximate the results of a Wright-Fisher model.

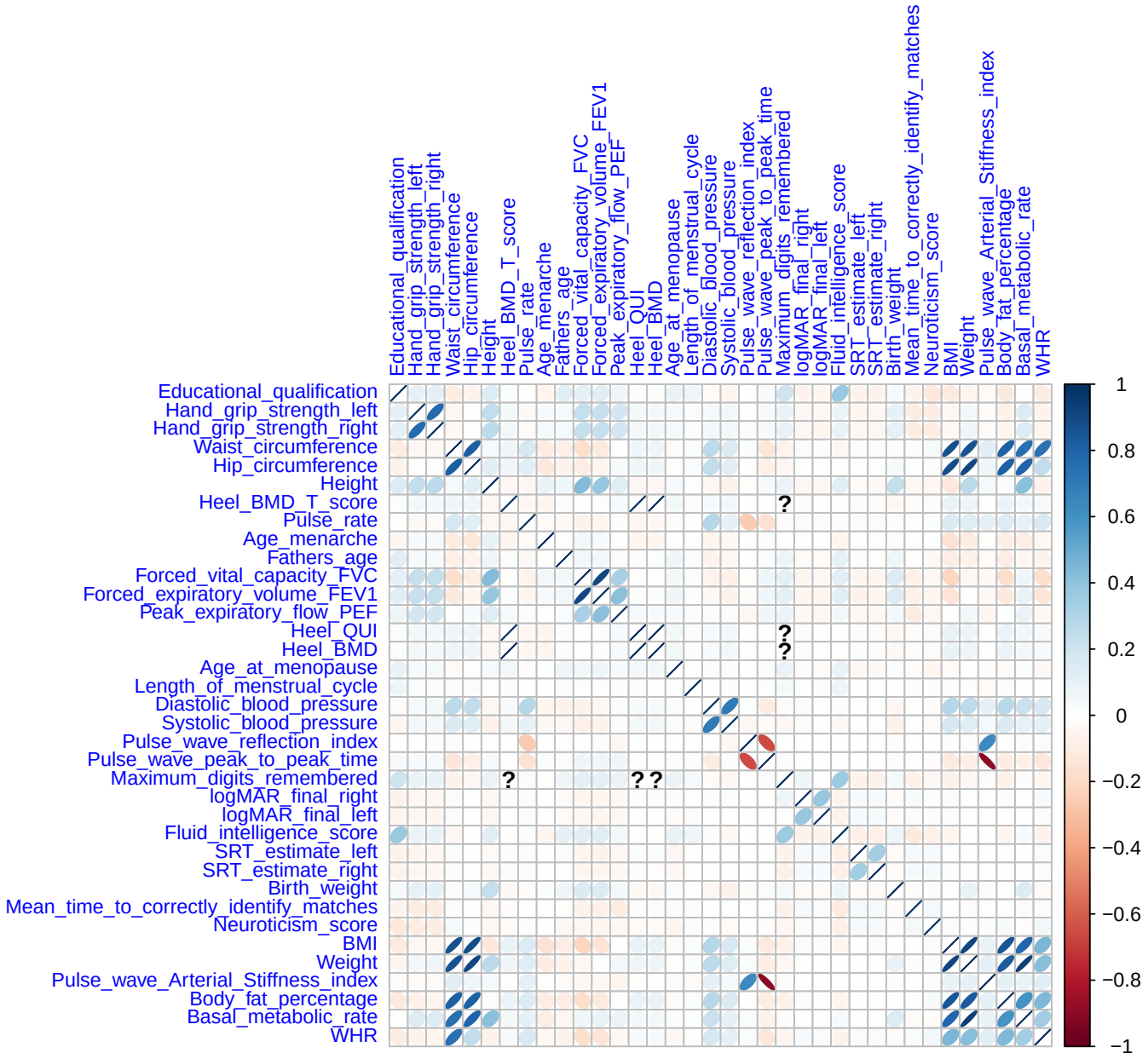

Fig. S4. Phenotypic correlation matrix for Females. Shows the correlation coefficient for the measured phenotypes in females. The color legend is shown on the right hand side, with dark blue and dark red representing strong positive and negative correlations, respectively.

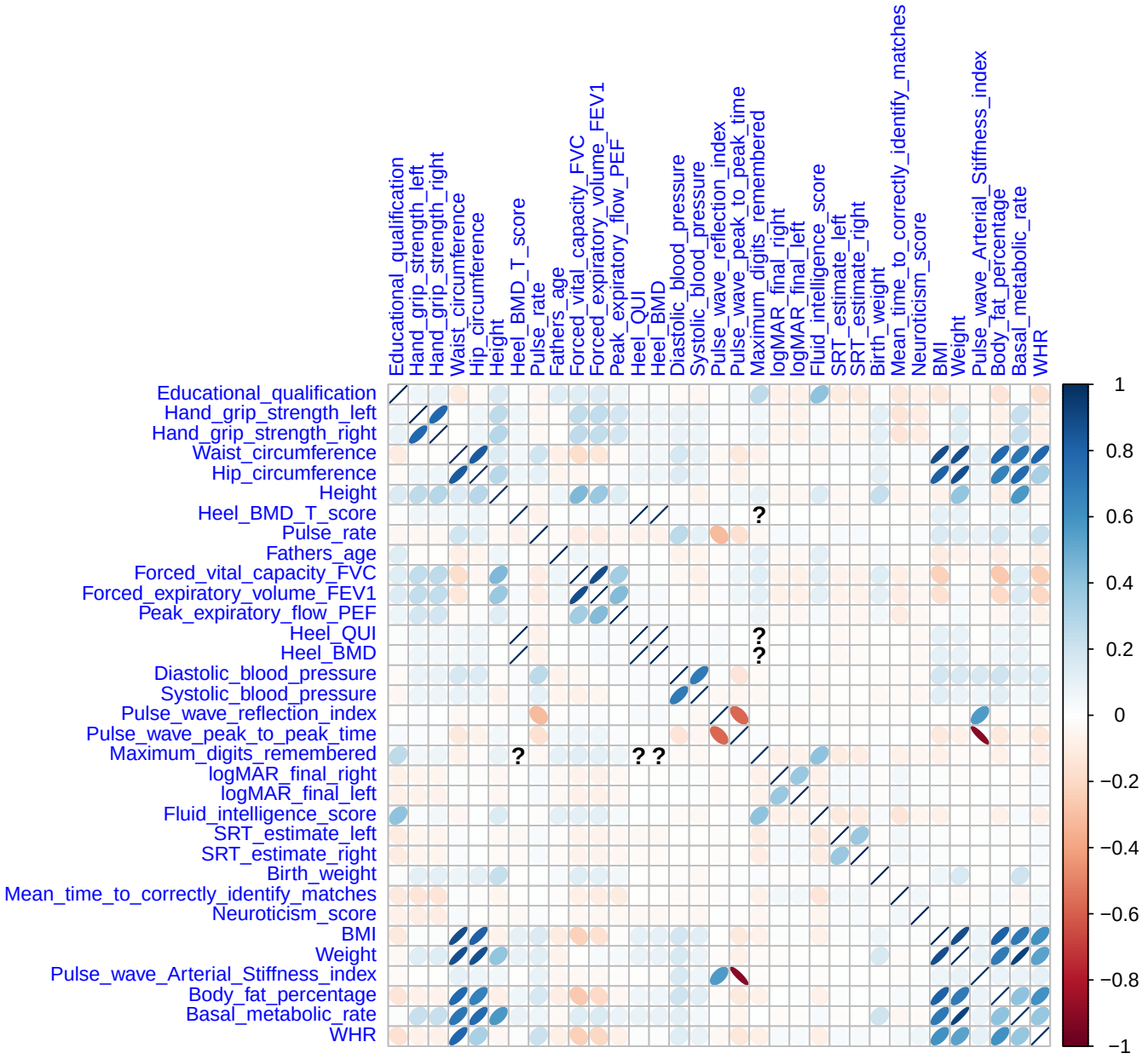

Fig. S5. Phenotypic correlation matrix for Males. Shows the correlation coefficient for the measured phenotypes in males. The color legend is shown on the right hand side, with dark blue and dark red representing strong positive and negative correlations, respectively.

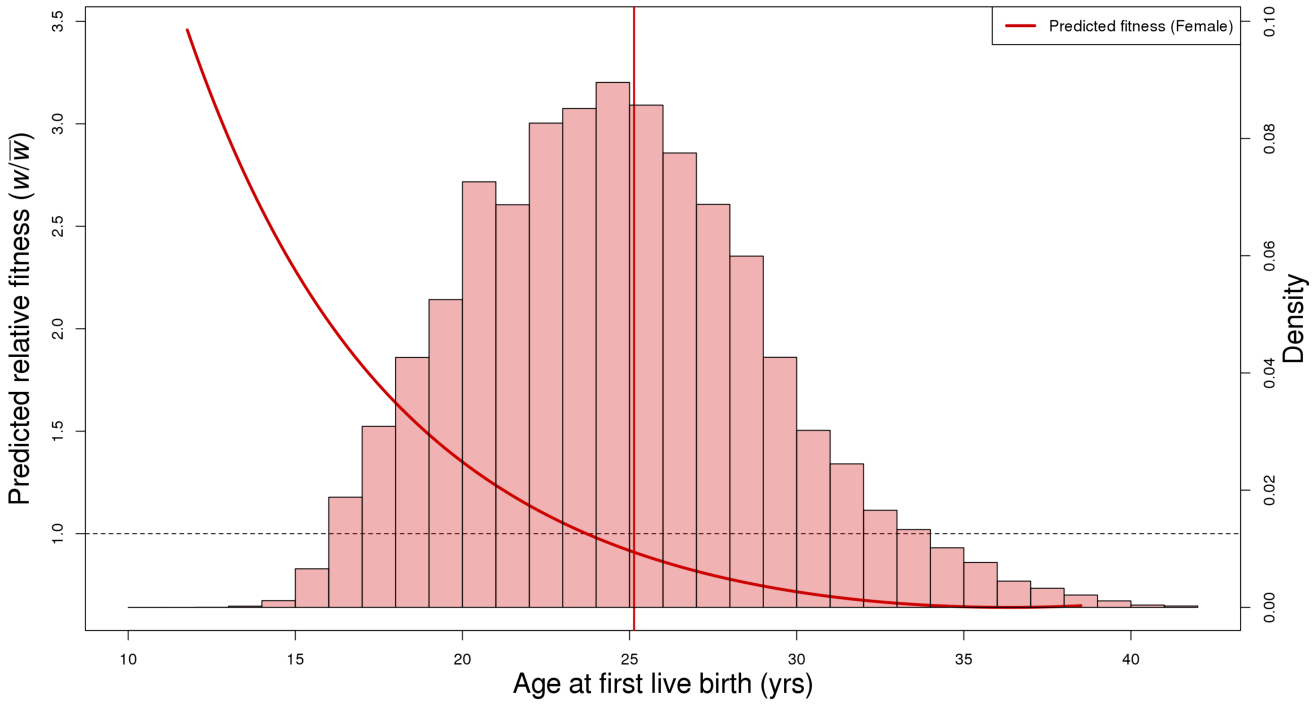

Fig. S6. Predicted relative fitness as a function of age at first live birth. Linear and quadratic selection gradients were converted into parameters of a Gaussian fitness function. Using the parameterized Gaussian fitness function, relative fitness values across the observed phenotypic range were predicted and shown by solid red (female) line. The population means are indicated by vertical solid red (female). Histograms of female (red) phenotypes are overlaid with an axis on the right hand side. The horizontal dashed line indicates a relative predicte fitness of 1.

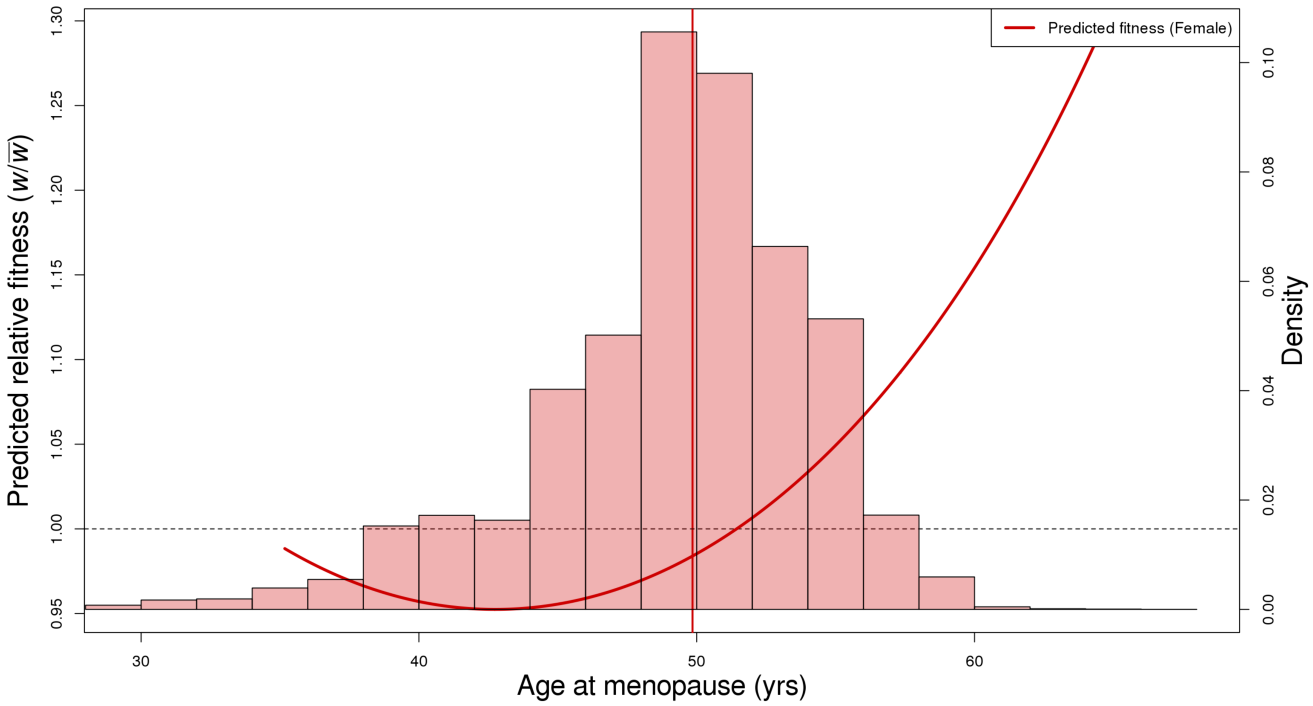

Fig. S7. Predicted relative fitness as a function of age at menopause. Linear and quadratic selection gradients were converted into parameters of a Gaussian fitness function. Using the parameterized Gaussian fitness function, relative fitness values across the observed phenotypic range were predicted and shown by solid red (female) line. The population means are indicated by vertical solid red (female). Histograms of female (red) phenotypes are overlaid with an axis on the right hand side. The horizontal dashed line indicates a relative predicted fitness of 1.

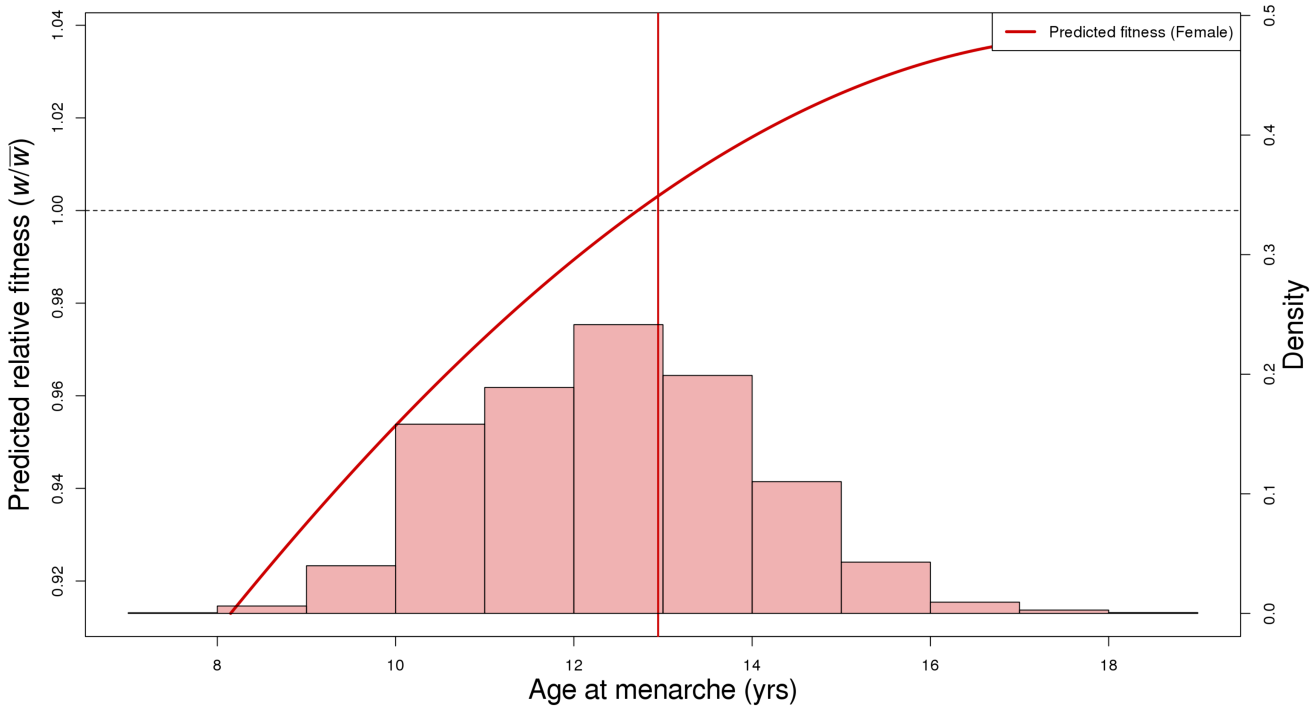

Fig. S8. Predicted relative fitness as a function of age at menarche. Linear and quadratic selection gradients were converted into parameters of a Gaussian fitness function. Using the parameterized Gaussian fitness function, relative fitness values across the observed phenotypic range were predicted and shown by solid red (female) line. The population means are indicated by vertical solid red (female). Histograms of female (red) phenotypes are overlaid with an axis on the right hand side. The horizontal dashed line indicates a relative predicted fitness of 1.

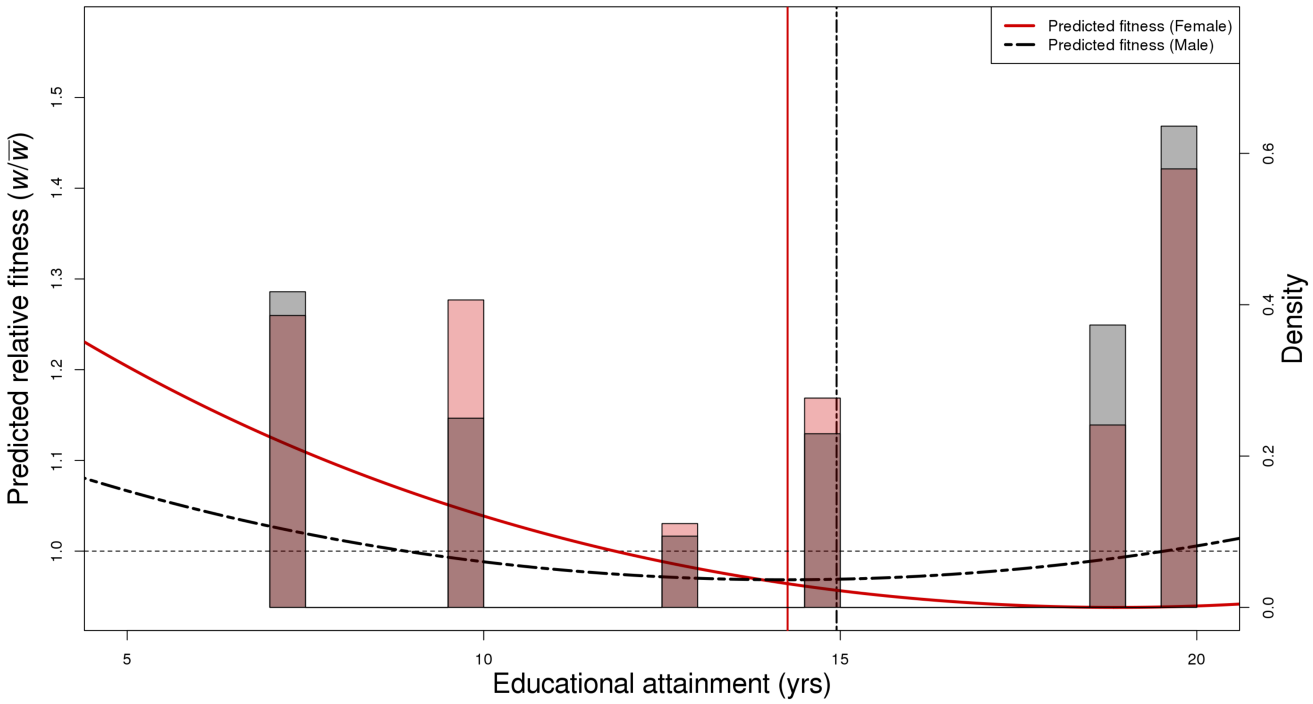

Fig. S9. Predicted relative fitness as a function of educational attainment. Linear and quadratic selection gradients were converted into parameters of a Gaussian fitness function. Using the parameterized Gaussian fitness function, relative fitness values across the observed phenotypic range were predicted and shown by solid red (female) and dashed black (male) lines. The population means are indicated by vertical solid red (female) and dashed black (male) lines. Histograms of female (red) and male (gray) phenotypes are overlaid with an axis on the right hand side. The horizontal dashed line indicates a relative predicted fitness of 1.

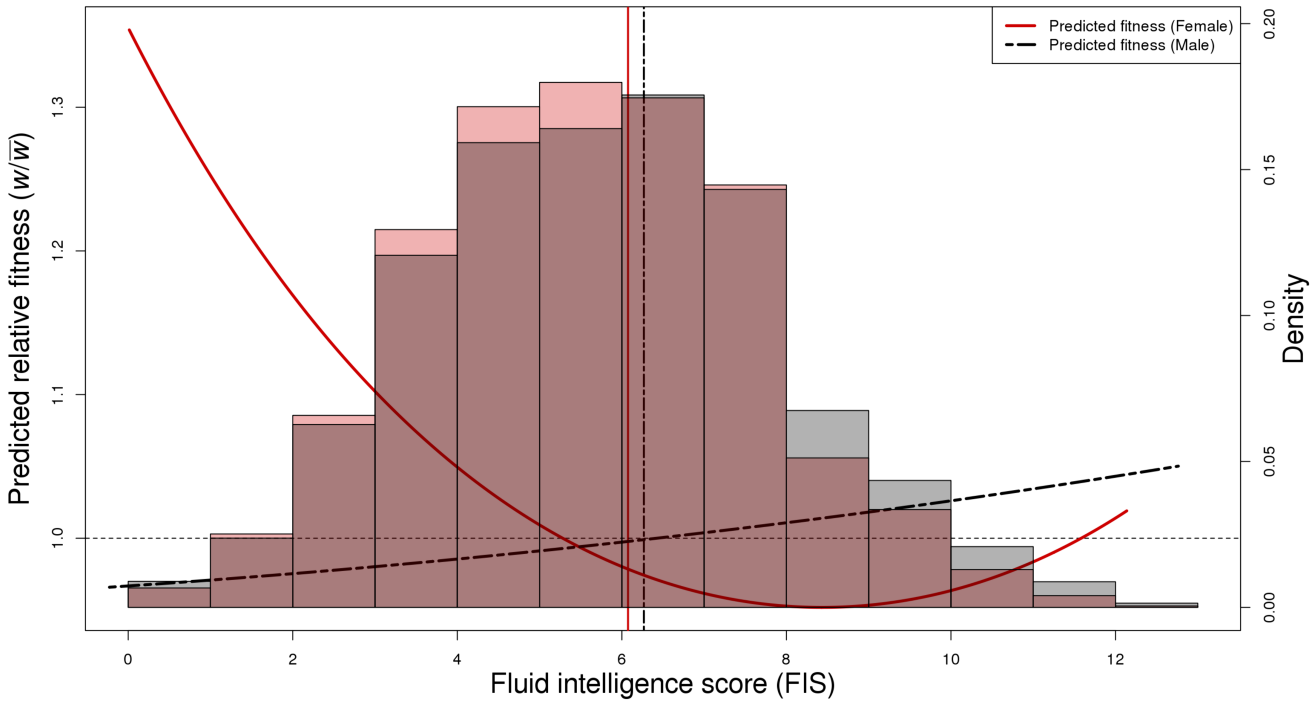

Fig. S10. Predicted relative fitness as a function of Fluid intelligence. Linear and quadratic selection gradients were converted into parameters of a Gaussian fitness function. Using the parameterized Gaussian fitness function, relative fitness values across the observed phenotypic range were predicted and shown by solid red (female) and dashed black (male) lines. The population means are indicated by vertical solid red (female) and dashed black (male) lines. Histograms of female (red) and male (gray) phenotypes are overlaid with an axis on the right hand side. The horizontal dashed line indicates a relative predicted fitness of 1.

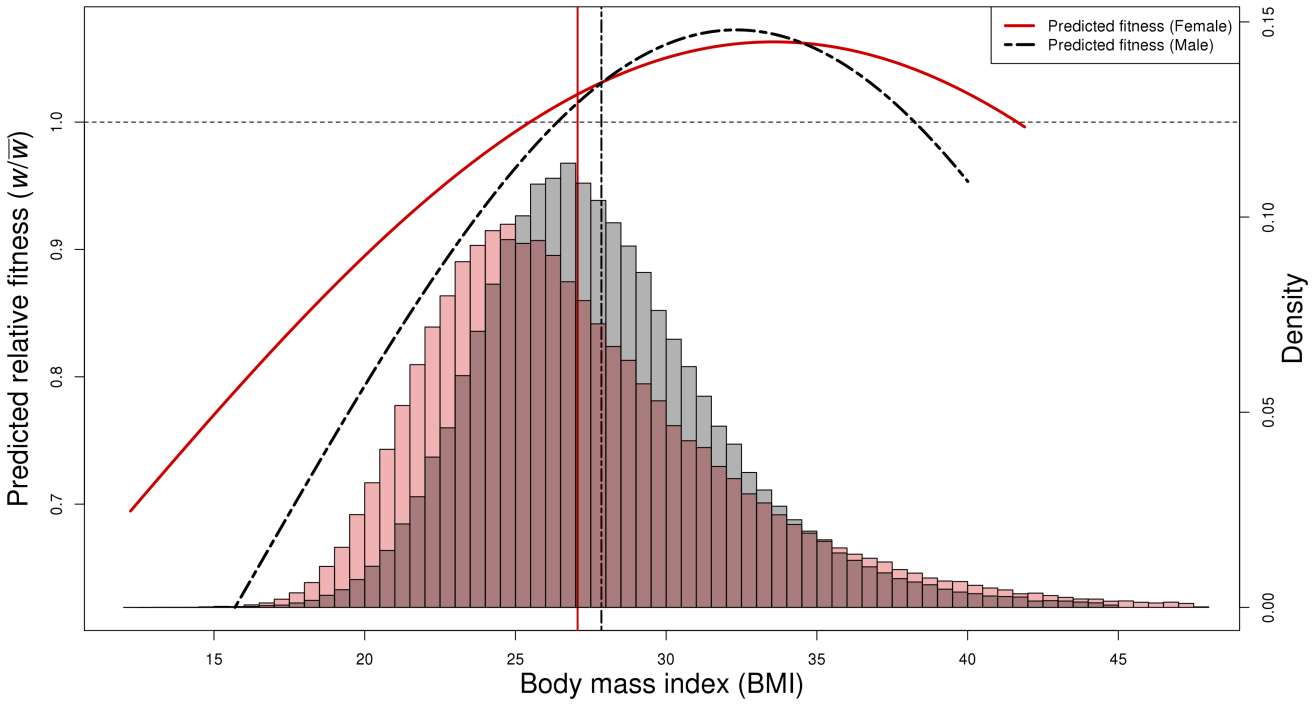

Fig. S11. Predicted relative fitness as a function of BMI. Linear and quadratic selection gradients were converted into parameters of a Gaussian fitness function. Using the parameterized Gaussian fitness function, relative fitness values across the observed phenotypic range were predicted and shown by solid red (female) and dashed black (male) lines. The population means are indicated by vertical solid red (female) and dashed black (male) lines. Histograms of female (red) and male (gray) phenotypes are overlaid with an axis on the right hand side. The horizontal dashed line indicates a relative predicted fitness of 1.

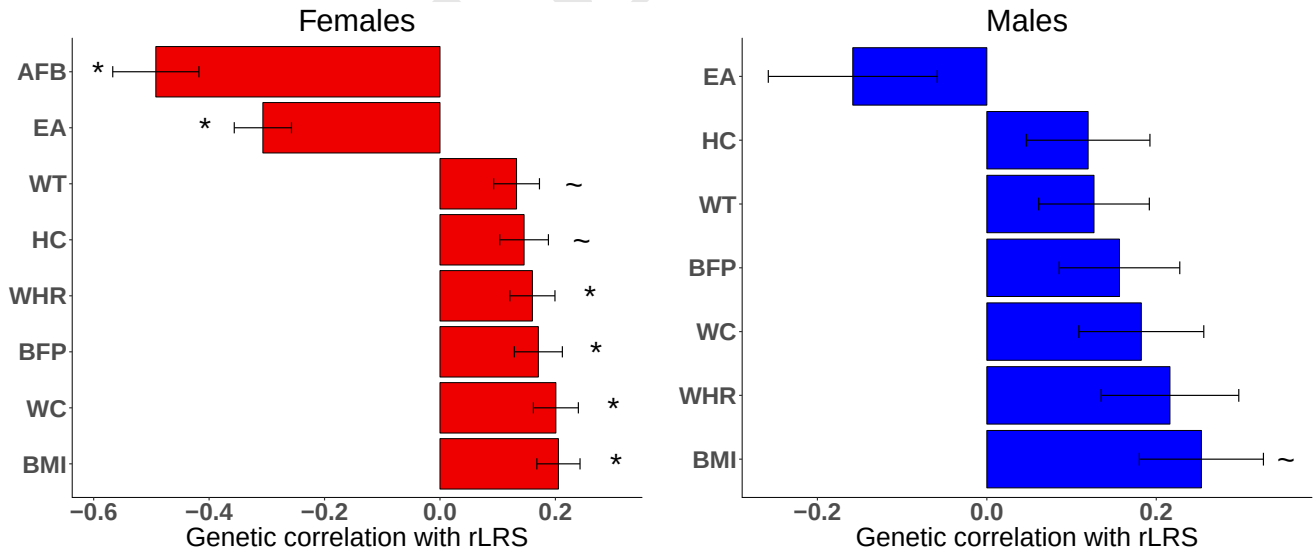

Fig. S12. Bar plots showing BOLT-REML estimates of genetic correlations between a selection of traits and rLRS for Females (red) and Males (blue) . Traits were selected on the basis of being marginally significant (p≤ 0.001) in at least one sex, and were sorted in ascending order of the estimate for each sex. Data are displayed as the correlation estimate plus or minus the standard error.($\sim p \leq 0.001$, *FWER≤ 0.05) Bars are labeled with abbreviated trait descriptions described in the text.

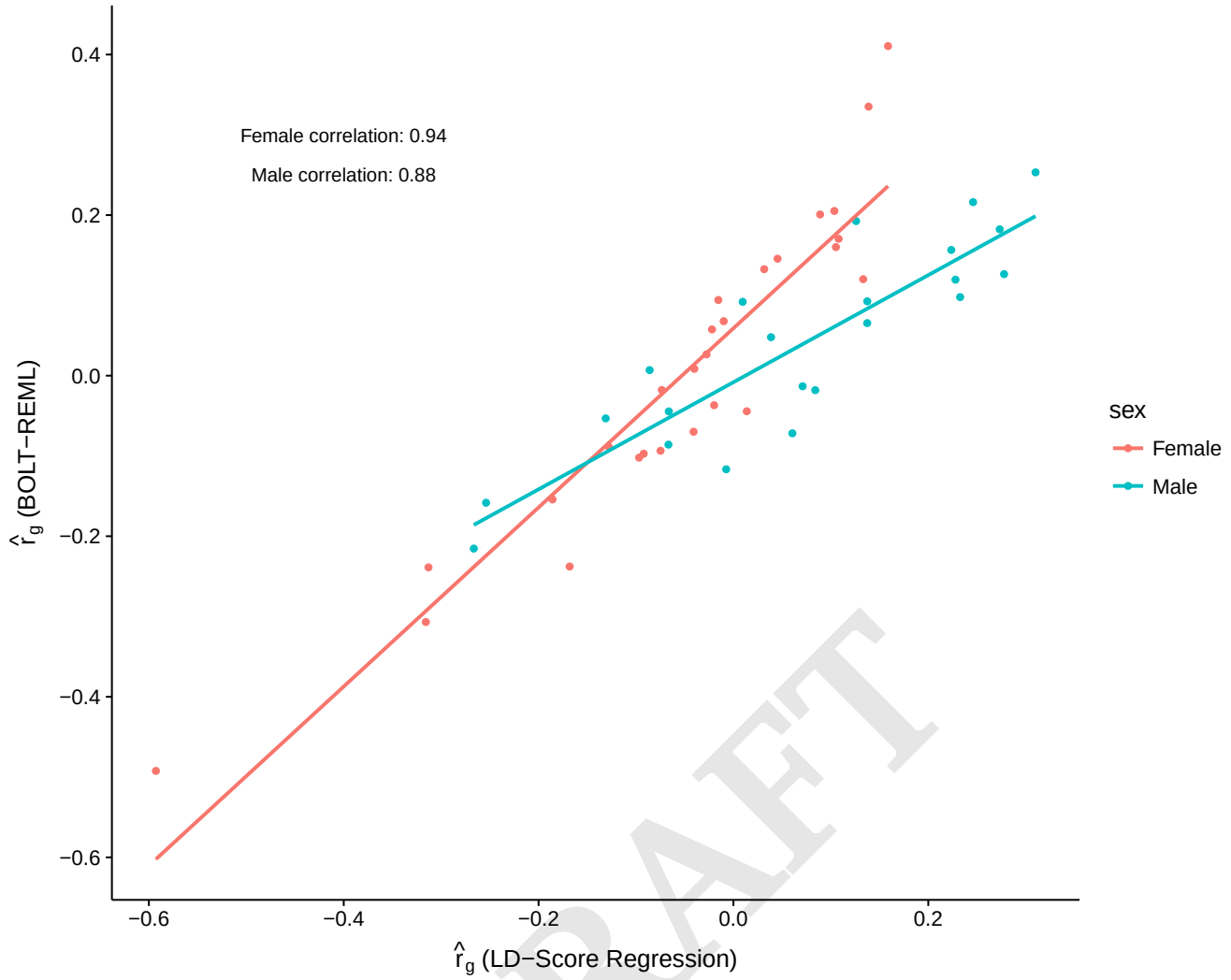

Fig. S13. Relationship between genetic correlation estimates. A scatter plot of the genetic correlation estimates from the UKB interim data release using a full REML approach versus genetic correlation estimates from the full UKB data release obtained from LD-score regression.

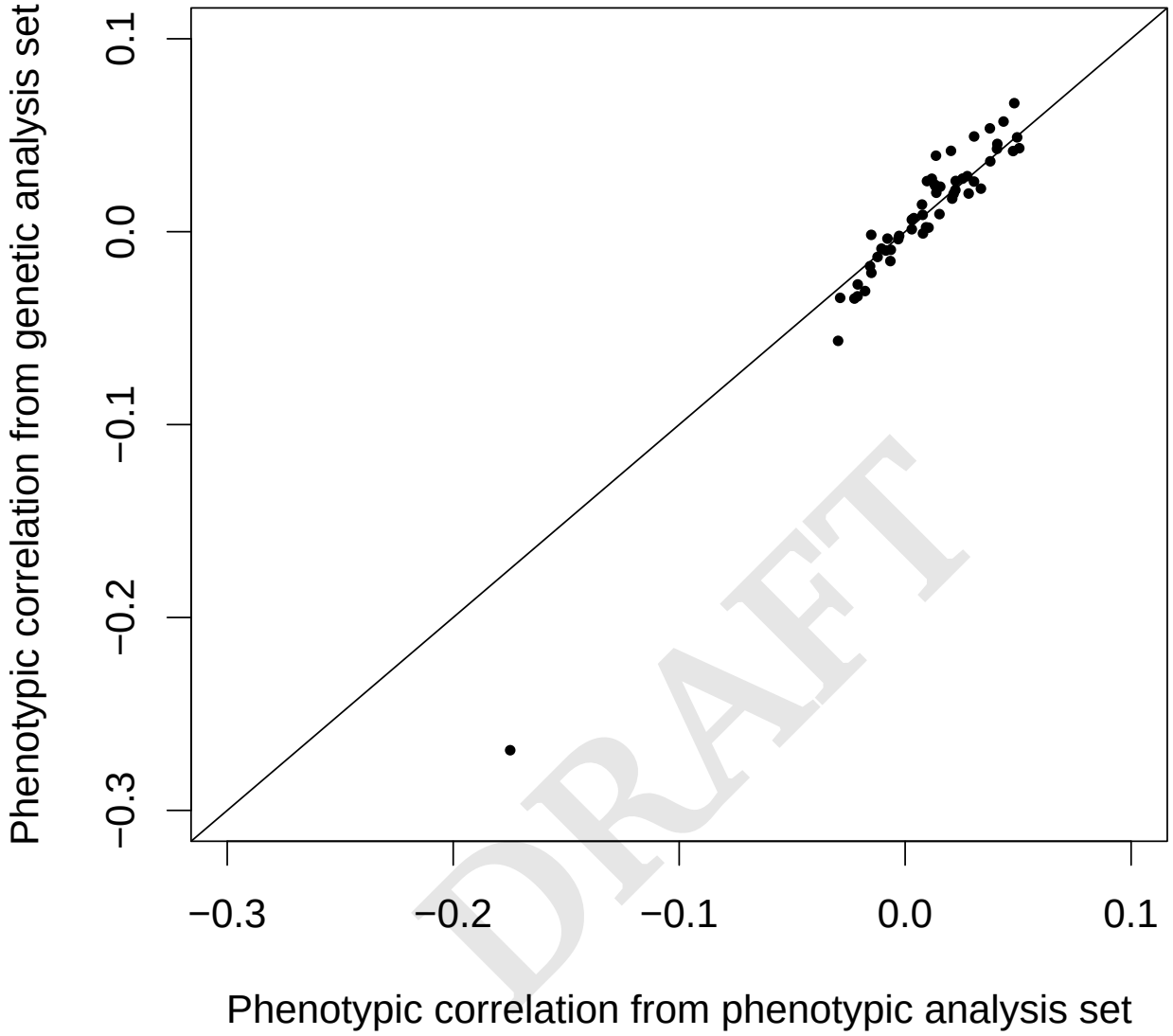

Fig. S14. Relationship between phenotypic correlation estimates. Phenotypic correlations are estimated from the phenotypic and genetic analyes($R^2 = 0.945$).

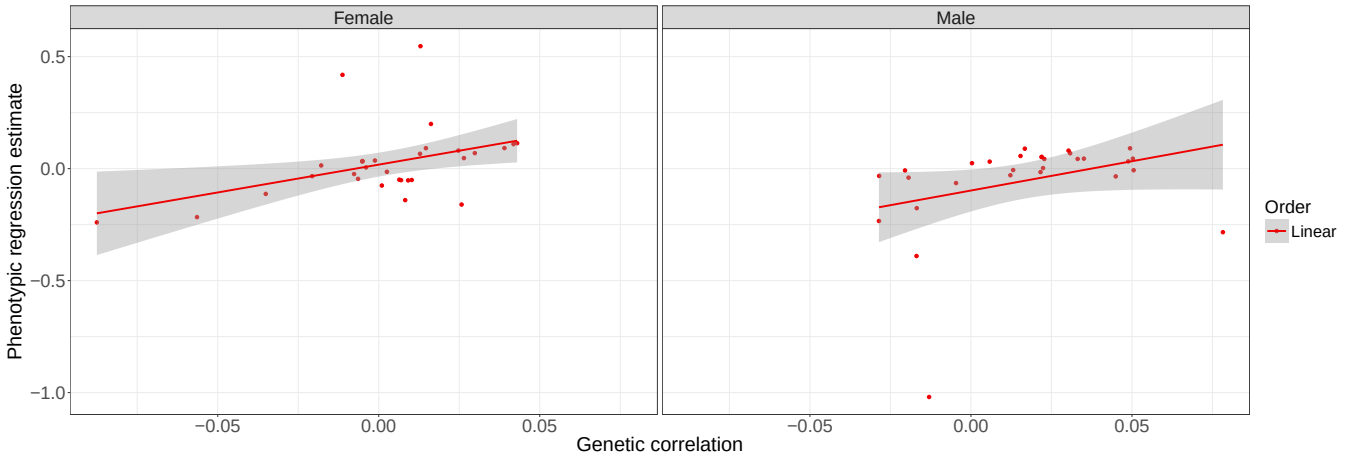

Fig. S15. Correlation between phenotypic regression estimates and genetic correlations. Phenotypic regression estimates and genetic correlations were grouped by sex and order. For females, there is significant correlation between phenotypic regressions and genetic correlations (Linear: $R^2 = 0.427, p < 10^{-4}$; Quadratic: $R^2 = 0.376$, $p = 0.0011$). For males,only the linear terms are marginally significantly correlated (Linear: $R^2 = 0.174, p = 0.014$; Quadratic: $R^2 = 0.092, p = 0.105$).

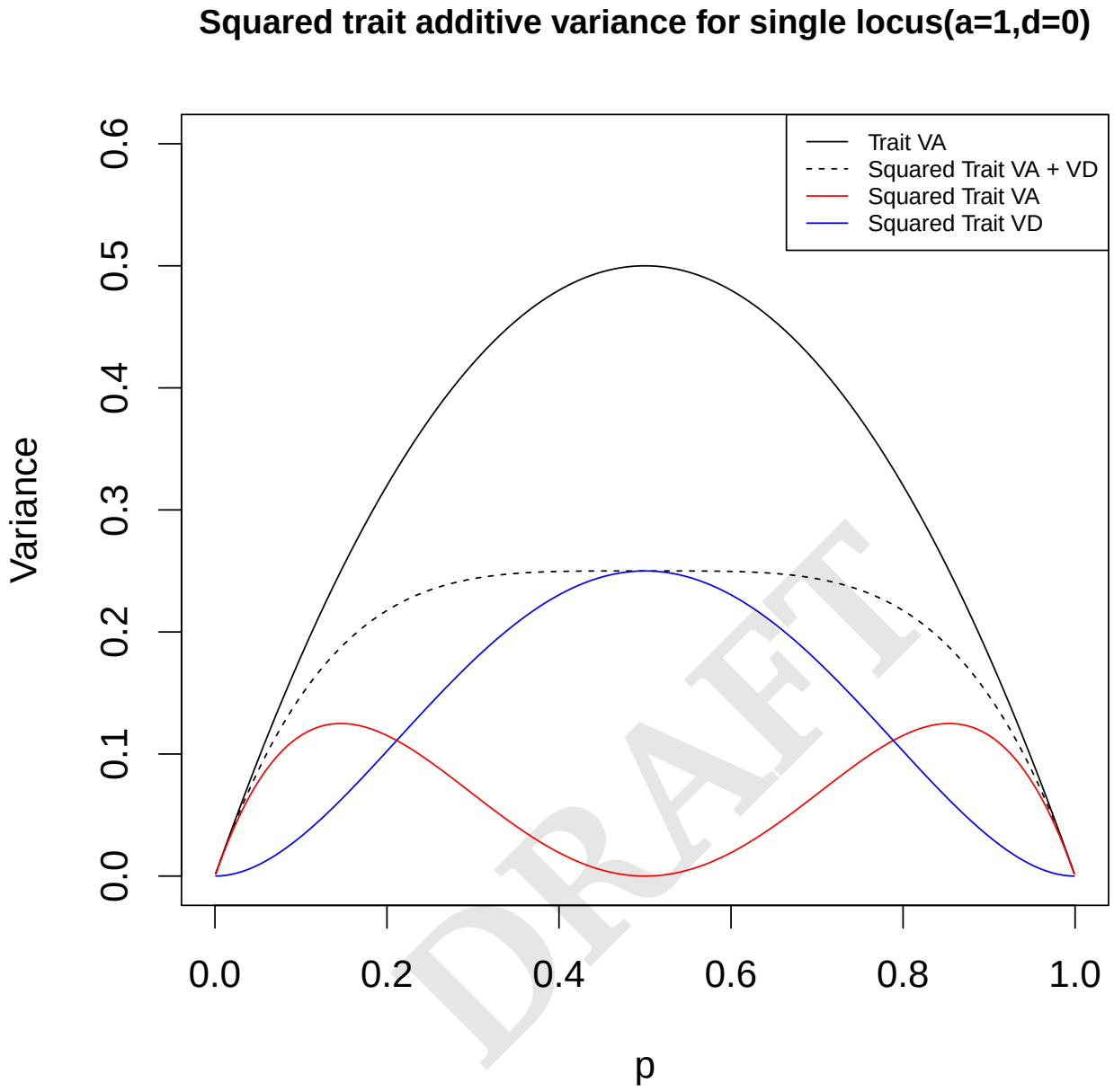

Fig. S16. Genetic variance for a squared trait determined by a single biallelic locus. In this case, the effect of the alleles is set to be $a = 1$.

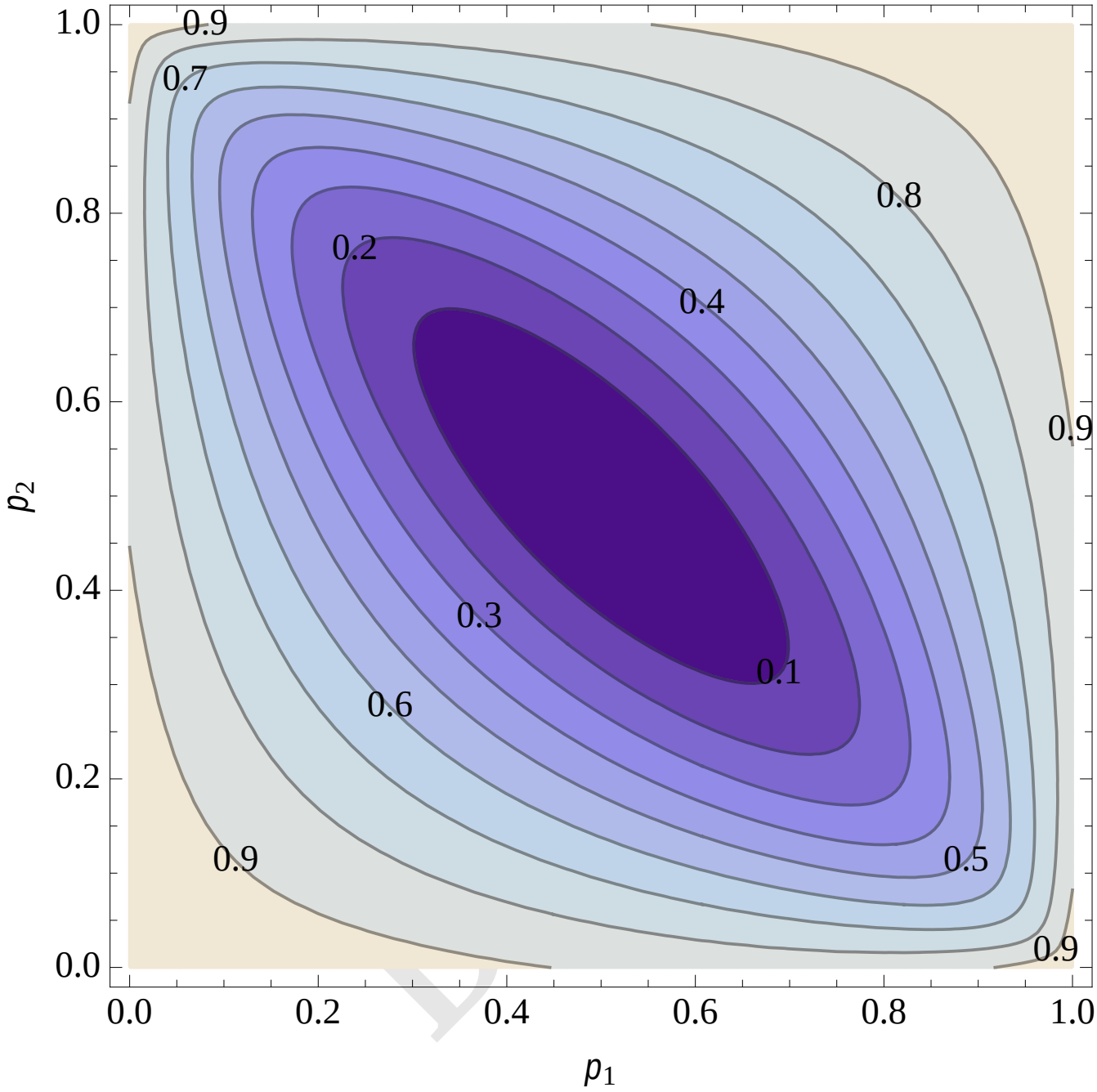

Fig. S17. The percentage of genetic variance for a squared trait which is purely additive. Under a purely additive two locus model with equal effects ($a = 1$), the squared trait contains additive, dominance and additive by additive epistatic variance components. The relative magnitudes of each component, depends on the allele frequencies. The axes represent allele frequencies at each locus and the color shows the relative magnitude of the additive variance component. Lighter colors show a large additive component.

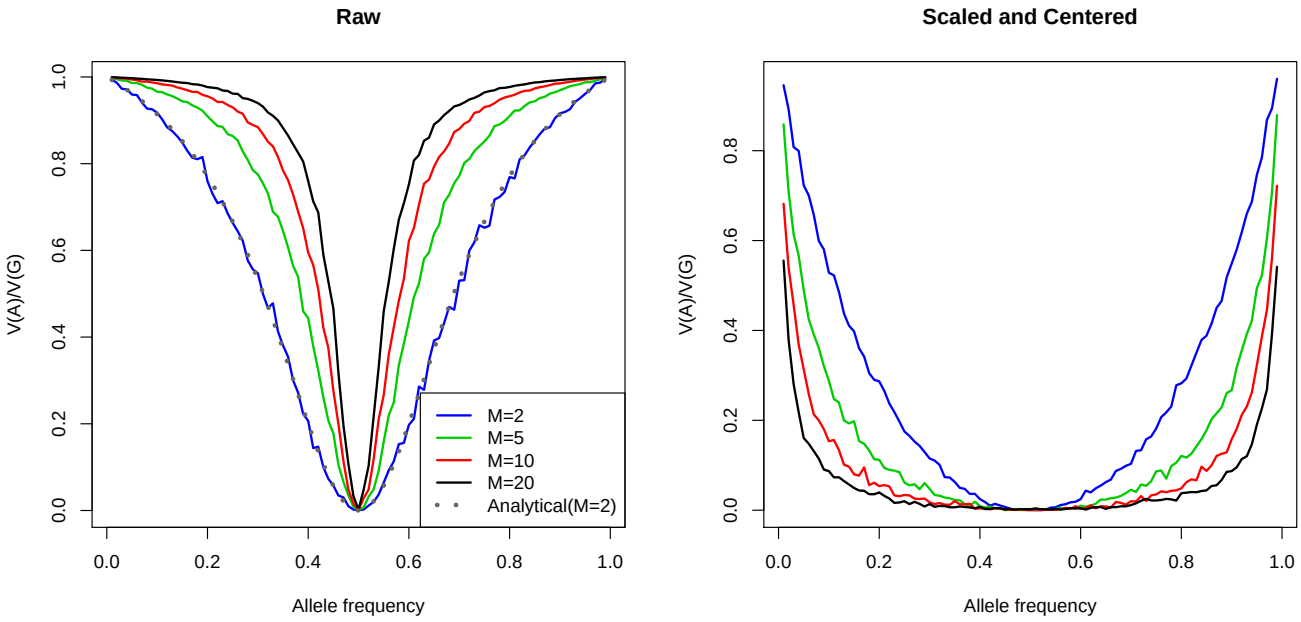

Fig. S18. Regression based estimates of the percentage of genetic variance for a squared trait which is purely additive, under a purely additive multilocus model with equal effects ($a = 1$). The regression was performed on the raw unscaled trait values (left) and the scaled(right) trait values. The number of markers was varied from M=2 to M=20. The analytic expression for M=2, which does not assume scaling, is displayed as a dotted line.

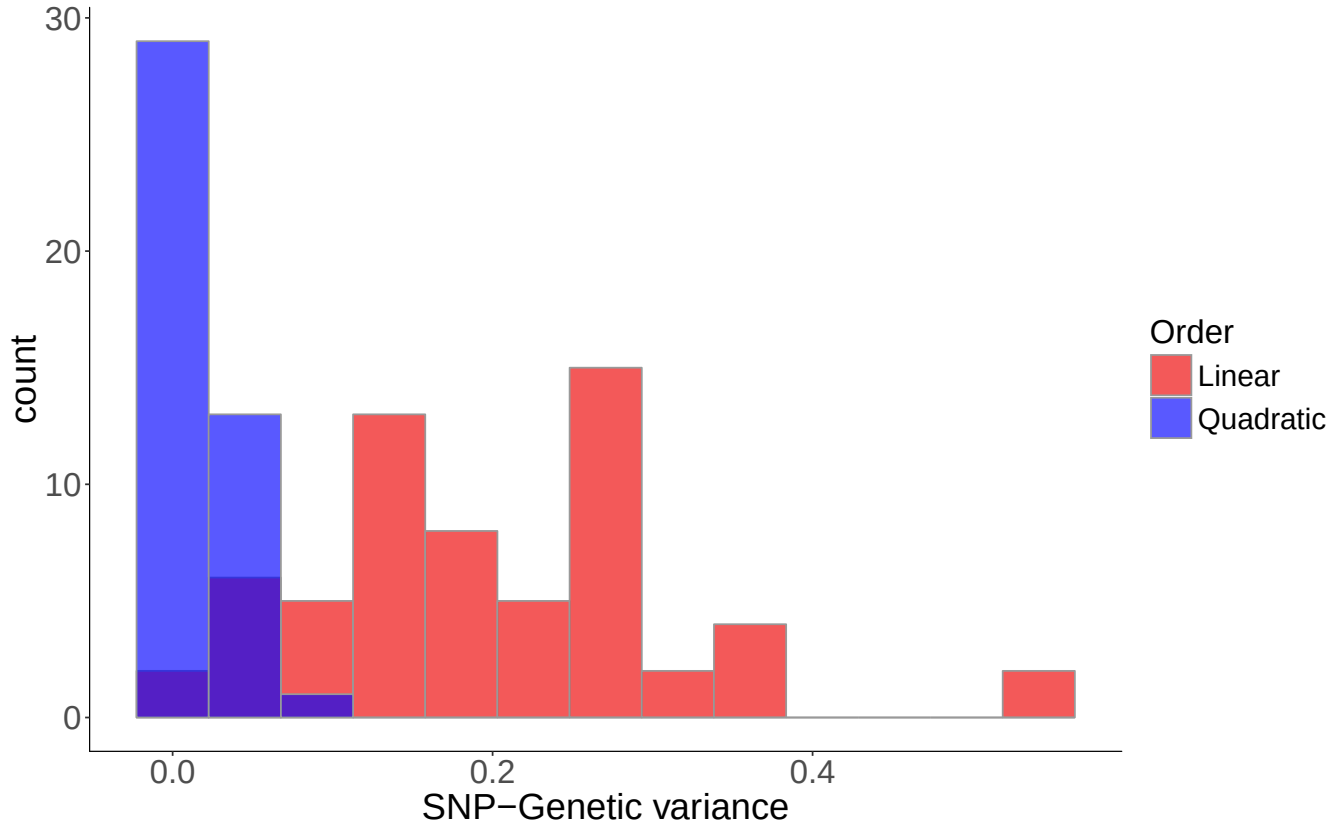

Fig. S19. The distribution of genetic variance explained by common SNPs. Estimates of genetic variance were for traits (red) and squared traits(blue) were obtained from the bivariate REML analysis in BOLT-LMM. The same samples were used in each case. Data for males and females were pooled here.

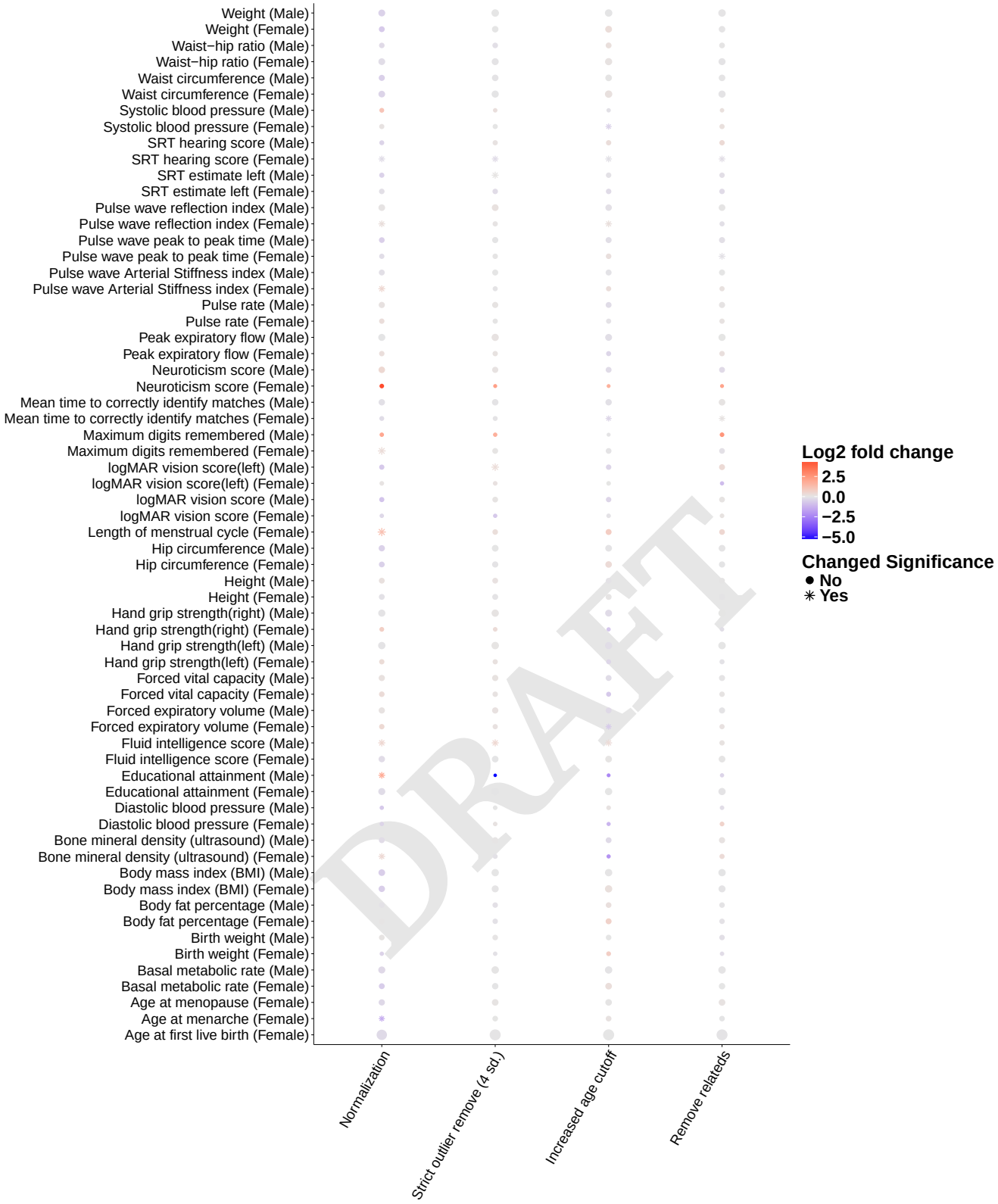

Fig. S20. Sensitivity analysis of linear selection gradients. Each set of β estimates is compared to a baseline analysis described in the the text. For each data QC pipeline we display the log fold-change in the value of β compared to and whether the estimate changed significance status. Red coloration implies that β increased in absolute magnitude and thus became more significant and vice versa for blue coloration.

Fig. S21. Sensitivity analysis of quadratic selection gradients. Each set of γ estimates is compared to a baseline analysis described in the the text. For each data QC pipeline we display the log fold-change in the value of γ compared to and whether the estimate changed significance status. Red coloration implies that γ increased in absolute magnitude and thus became more significant and vice versa for blue coloration.

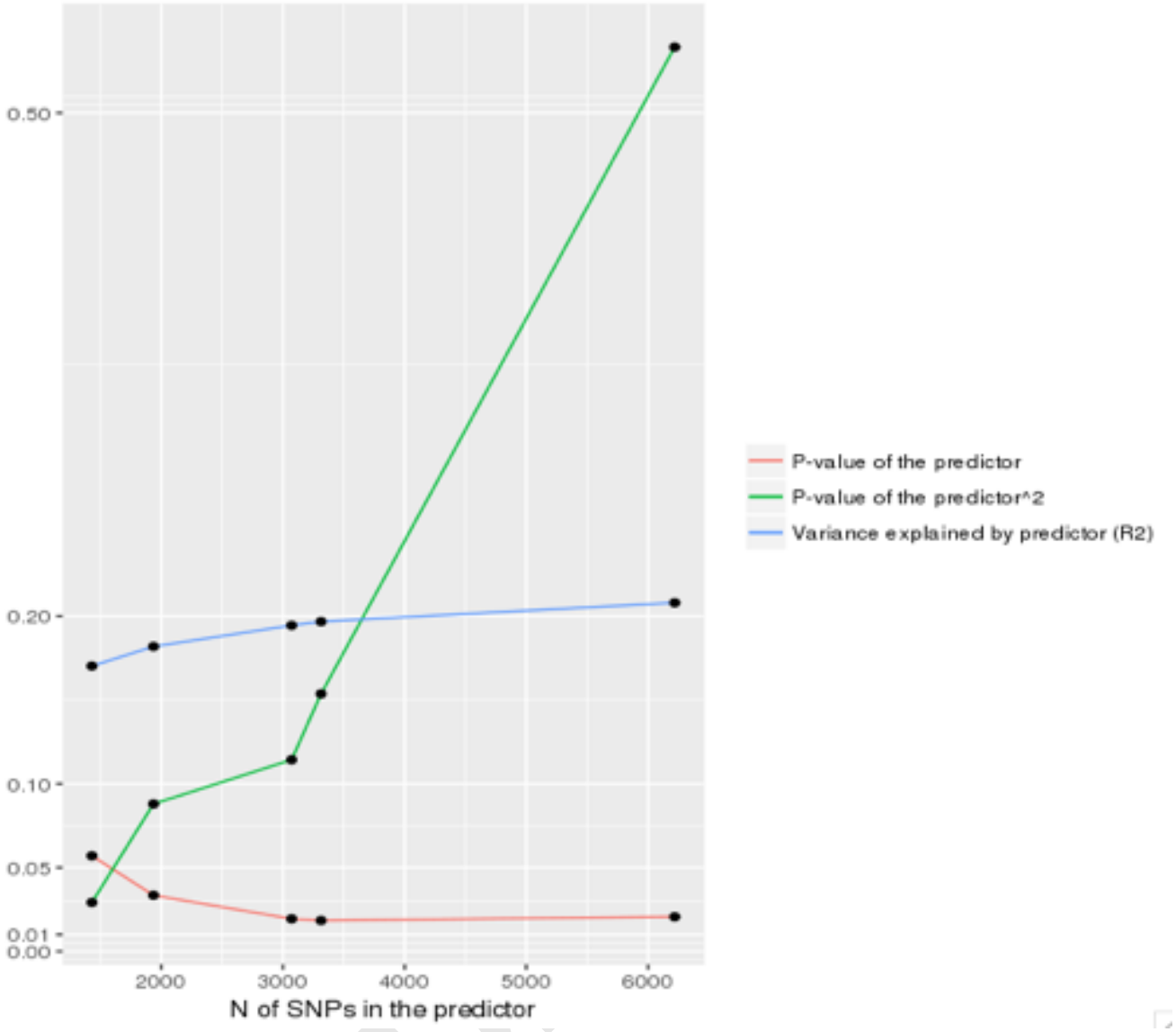

Fig. S22. Performance of polygenic predictor for height. Polygenic predictors for height and squared height were constructed based on genetic association statistics obtained from a meta-analysis of the UKB and GIANT data. The R^2 score and p-values for each predictor are plotted against the number of SNPs included in the model.

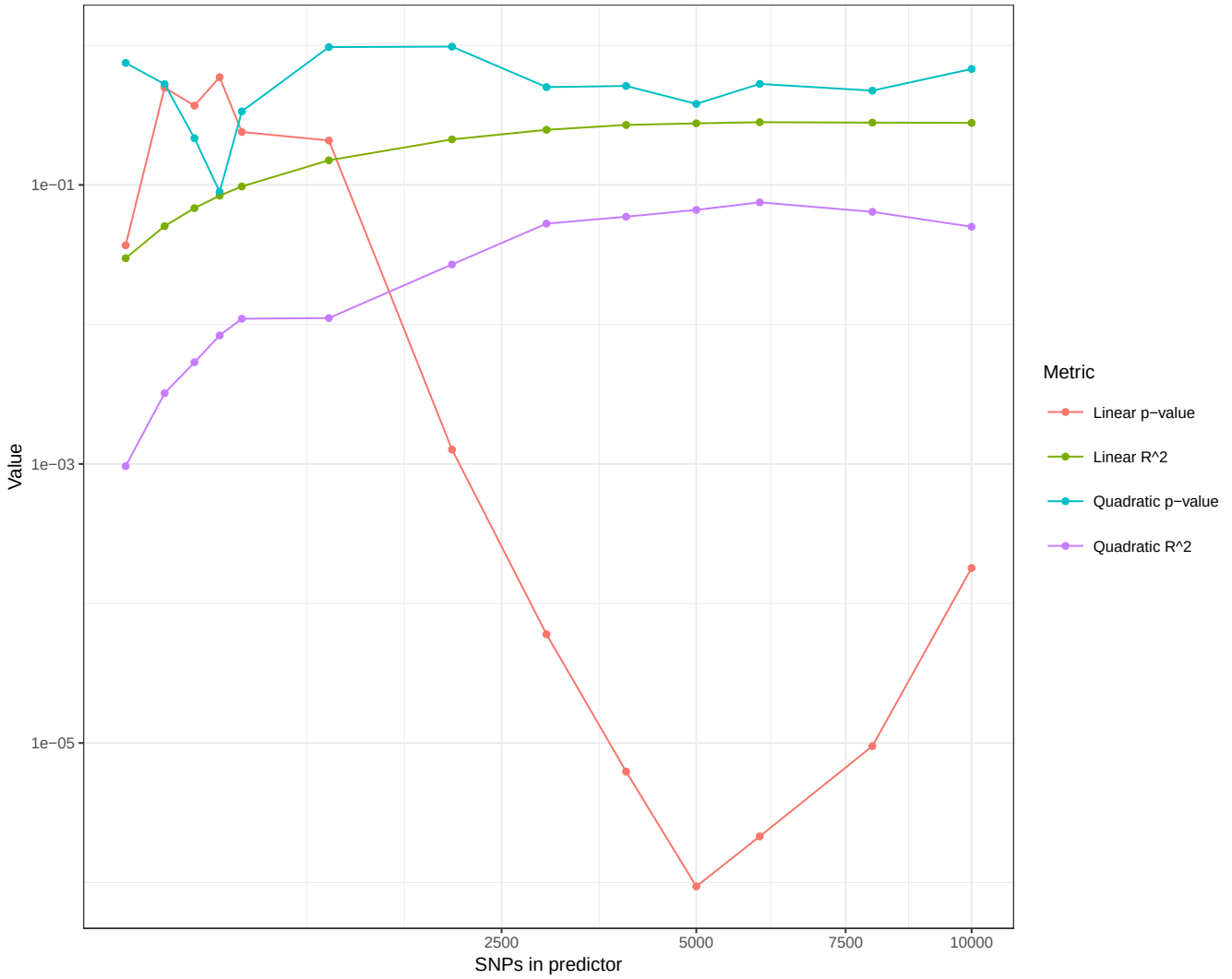

Fig. S23. Performance of simulated polygenic predictors. A phenotype was simulated under a polygenic model with 20,000 causal markers. SNP effects were estimate in a discovery panel of 300,000 individuals. Polygenic predictors for the phenotype and squared phenotype were constructed in a test panel of 50,000 individuals. The R^2 score and p-values for each predictor are plotted against the number of SNPs included in the model.

SI Tables.

Table S1. Summary of multiple regression of traits onto rLRS. Traits which were marginally significant in a multiple regression model are displayed below. The multiple regression was carried out separately for each sex. The full results of multiple regression are contained in the Dataset S1.

Trait	Sex	Order	Estimate	$-log_{10}(p)$
Educational attainment	Female	1	0.04	23
Age at menarche	Female	1	0.02	4
Age at first live birth	Female	1	-0.18	>220
Bone mineral density (ultrasound)	Female	1	-0.02	5
Systolic blood pressure	Female	1	-0.03	8
Waist-hip ratio	Female	1	0.04	14
Hand grip strength(right)	Male	1	0.05	15
Pulse rate	Male	1	-0.04	7
Systolic blood pressure	Male	1	-0.03	4
Body mass index (BMI)	Male	1	0.08	17
Age at first live birth	Female	2	0.04	43
Body mass index (BMI)	Female	2	0.01	5
Educational attainment	Male	2	0.05	6
Body mass index (BMI)	Male	2	-0.03	13

Table S2. Summary of multiple regression of educational attainment and age at first birth onto rLRS. The linear model $rLRA\ EA + AFB + EA * AFB + \epsilon$ was fit to the female samples. Both predictors as well as their interaction term were found to be statistically significant.

Predictor	Estimate	$-log10(p)$
Educational Attainment (EA)	0.032	75
Age at First Birth (AFB)	0.167	> 220
Interaction (EA:AFB)	0.038	112

SI Datasets.

Dataset S1. Supplemental excel file containing simple and multiple regression results.

Dataset S2. Supplemental text file containing genetic correlation results.

References.

1. Sudlow C, et al. (2015) UK Biobank: An Open Access Resource for Identifying the Causes of a Wide Range of Complex Diseases of Middle and Old Age. *PLoS Medicine* 12(3).
2. Beauchamp JP (2016) Genetic evidence for natural selection in humans in the contemporary United States. *Proceedings of the National Academy of Sciences of the United States of America* 113(28):7774–7779.
3. Yang J, Lee SH, Goddard ME, Visscher PM (2011) GCTA: a tool for genome-wide complex trait analysis. *American journal of human genetics* 88(1):76–82.
4. Lande R, Arnold S (1983) The measurement of selection on correlated characters. *Evolution* 37(6):1210–1226.
5. Stinchcombe JR, Agrawal AF, Hohenlohe PA, Arnold SJ, Blows MW (2008) Estimating nonlinear selection gradients using quadratic regression coefficients: double or nothing? *Evolution* 62(9):2435–40.
6. Bulik-Sullivan BK, et al. (2015) LD Score regression distinguishes confounding from polygenicity in genome-wide association studies. *Nature Genetics* 47(3):291–295.

7. Bulik-Sullivan B, et al. (2015) An atlas of genetic correlations across human diseases and traits. *Nature Genetics* 47(11):1236–1241.
8. Purcell S, et al. (2007) PLINK: a tool set for whole-genome association and population-based linkage analyses. *American journal of human genetics* 81(3):559–75.
9. Loh PR, et al. (2015) Contrasting genetic architectures of schizophrenia and other complex diseases using fast variance-components analysis. *Nature Genetics* 47(12):1385–1392.
10. Yang J, et al. (2012) FTO genotype is associated with phenotypic variability of body mass index. *Nature* 490(7419):267–272.
11. Tropf FC, et al. (2015) Human fertility, molecular genetics, and natural selection in modern societies. *PLoS One* 10(6):e0126821.
12. Thompson R (1973) The Estimation of Variance and Covariance Components with an Application when Records are Subject to Culling. *Biometrics* 29(3):527.
13. Lee SH, Yang J, Goddard ME, Visscher PM, Wray NR (2012) Estimation of pleiotropy between complex diseases using single-nucleotide polymorphism-derived genomic relationships and restricted maximum likelihood. *Bioinformatics (Oxford, England)* 28(19):2540–2.
14. Burger RR (2000) *The mathematical theory of selection, recombination, and mutation*. (Wiley), p. 409.
15. Zhu Z, et al. (2017) Causal associations between risk factors and common diseases inferred from GWAS summary data. *doi.org* p. 168674.
16. Okbay A, et al. (2016) Genome-wide association study identifies 74 loci associated with educational attainment. *Nature* 533(7604):539–542.
17. Kojima K (1959) Role of Epistasis and Overdominance in Stability of Equilibriea with Selection. *Proceedings of the National Academy of Sciences of the United States of America* 45(7):984–9.
18. Mäki-Tanila A, Hill WG (2014) Influence of gene interaction on complex trait variation with multilocus models. *Genetics* 198(1):355–67.
19. Slatkin M, Lande R (1976) Niche Width in a Fluctuating Environment-Density Independent Model. *The American Naturalist* 110(971):31–55.
20. Bull JJ (1987) Evolution of Phenotypic Variance. *Evolution* 41(2):303.
21. Zhang XS, Hill WG (2005) Evolution of the environmental component of the phenotypic variance: stabilizing selection in changing environments and the cost of homogeneity. *Evolution* 59(6):1237–44.
22. Zhang X, Hill WG (2008) Mutation-Selection Balance for Environmental Variance. *The American Naturalist* 171(3):394–399.
23. Hill WG, Mulder HA (2010) Genetic analysis of environmental variation. *Genetics Research* 92(5-6):381–395.
24. Visscher PM, Posthuma D (2010) Statistical Power to Detect Genetic Loci Affecting Environmental Sensitivity. *Behavior Genetics* 40(5):728–733.

Table S3. Summary of correlation coefficients. This table contains the calculated phenotypic, genetic, and residual correlations from the analyses presented in the main text. Columns correspond to the genetic correlation from LD score regression $r_{g,LDSC}$, phenotypic correlation from regression analyses $r_{p,full}$, the phenotypic correlation from mixed model analyses $r_{p,BOLT}$, the genetic correlation from mixed model analyses $r_{g,BOLT}$, and the residual correlation from the mixed model $r_{e,BOLT}$. Note that these are correlation coefficients not covariances and are thus normalized by total variance components. This means that the residual correlation can be smaller than the genetic correlation but still have a greater contribution to the phenotypic correlation if the residual variances are larger than the genetic variance explained by genotyped SNPs.

Predictor	Sex	$r_{g,LDSC}$	$r_{p,full}$	$r_{p,BOLT}$	$r_{g,BOLT}$	$r_{e,BOLT}$
Age at first live birth	Female	-0.593	-0.175	-0.269	-0.492	-0.254
Age at menopause	Female	-0.168	0.028	0.020	-0.238	0.052
Age at menarche	Female	0.133	0.013	0.024	0.120	0.008
Basal metabolic rate	Female	-0.015	0.025	0.028	0.094	0.016
Birth weight	Female	-0.073	0.003	0.001	-0.018	0.003
Body mass index (BMI)	Female	0.104	0.038	0.036	0.205	0.009
Body fat percentage	Female	0.108	0.012	0.027	0.170	0.004
Diastolic blood pressure	Female	-0.022	-0.003	-0.004	0.058	-0.013
Fluid intelligence score	Female	-0.313	-0.030	-0.057	-0.239	-0.032
Forced expiratory volume	Female	-0.075	0.008	-0.001	-0.094	0.015
Forced vital capacity	Female	-0.092	0.010	0.002	-0.097	0.020
Hand grip strength(right)	Female	-0.097	0.003	0.006	-0.102	0.019
Bone mineral density (ultrasound)	Female	-0.010	-0.007	-0.015	0.068	-0.035
Height	Female	-0.128	-0.018	-0.031	-0.089	-0.019
Hip circumference	Female	0.045	0.022	0.026	0.146	0.008
Maximum digits remembered	Female	-0.028	-0.016	-0.018	0.027	-0.022
Mean time to correctly identify matches	Female	0.014	-0.006	-0.009	-0.044	-0.007
Peak expiratory flow	Female	-0.041	0.009	0.002	-0.070	0.011
Pulse rate	Female	-0.020	-0.009	-0.010	-0.037	-0.006
Pulse wave Arterial Stiffness index	Female	-0.186	0.007	0.014	-0.154	0.026
Pulse wave peak to peak time	Female	0.159	-0.010	-0.009	0.411	-0.039
SRT hearing score	Female	0.139	0.010	0.026	0.335	0.015
Systolic blood pressure	Female	-0.040	-0.008	-0.004	0.009	-0.005
Waist circumference	Female	0.089	0.041	0.043	0.201	0.019
Weight	Female	0.032	0.028	0.029	0.133	0.012
Waist-hip ratio	Female	0.105	0.037	0.054	0.160	0.038
Basal metabolic rate	Male	0.233	0.050	0.049	0.098	0.048
Birth weight	Male	0.071	0.014	0.020	-0.013	0.023
Body mass index (BMI)	Male	0.310	0.048	0.042	0.253	0.020
Body fat percentage	Male	0.224	0.013	0.024	0.157	0.010
Diastolic blood pressure	Male	0.137	0.004	0.007	0.065	0.003
Forced expiratory volume	Male	-0.086	0.022	0.022	0.007	0.025
Forced vital capacity	Male	-0.066	0.021	0.020	-0.045	0.028
Hand grip strength(right)	Male	0.060	0.044	0.057	-0.072	0.069
Bone mineral density (ultrasound)	Male	0.126	0.021	0.017	0.193	0.003
Height	Male	-0.007	0.015	0.009	-0.117	0.038
Hip circumference	Male	0.228	0.034	0.022	0.120	0.013
Mean time to correctly identify matches	Male	-0.131	-0.029	-0.034	-0.053	-0.033
Neuroticism score	Male	-0.067	-0.021	-0.033	-0.086	-0.031
Peak expiratory flow	Male	0.009	0.041	0.046	0.092	0.043
Pulse rate	Male	0.084	-0.021	-0.027	-0.018	-0.029
Pulse wave Arterial Stiffness index	Male	0.137	0.020	0.042	0.093	0.038
Pulse wave peak to peak time	Male	-0.267	-0.022	-0.035	-0.215	-0.024
Systolic blood pressure	Male	0.039	-0.003	-0.002	0.048	-0.006
Waist circumference	Male	0.273	0.030	0.026	0.182	0.010
Weight	Male	0.278	0.050	0.043	0.126	0.036
Waist-hip ratio	Male	0.246	0.016	0.023	0.216	0.005